INTERNATIONAL JOURNAL FOR NUMERICAL METHODS IN ENGINEERING
Int. J. Numer. Meth. Engng 2002; **54**:263–297 (DOI: 10.1002/nme.426)

A contact formulation based on localized Lagrange multipliers: formulation and application to two-dimensional problems

G. Rebel, K. C. Park*,† and C. A. Felippa

Center for Aerospace Structures and Department of Aerospace Engineering Sciences, University of Colorado at Boulder, Campus Box 429, Boulder, CO 80309-0429, U.S.A.

SUMMARY

The non-penetration condition in contact problems is traditionally based on the classical Lagrange multiplier method. This method makes extensive use of modelling details of the contacting bodies for contact enforcement as the contact surface meshes are in general non-matching. To deal with this problem we introduce a novel element in the Lagrange multiplier approach of contact modelling, namely, a contact frame placed in between contacting bodies. It acts as a medium through which contact forces are transferred without violating equilibrium in the contact domain for discrete contact models. Only nodal information of the contacting bodies is required which makes the proposed contact enforcement generic. The contact frame has its own independent freedoms, which allows the formulation to pass contact patch tests by design. Copyright © 2002 John Wiley & Sons, Ltd.

KEY WORDS: finite element method; contact frame; localised Lagrange multipliers

1. INTRODUCTION

The computational modelling and analysis of structural contact problems have been important subjects of interest over the past several decades. Traditionally, the non-penetration condition has been enforced exactly by the Lagrange multiplier technique [1–5] or approximately by a penalty method [6, 7, 5]. The traditional Lagrange multiplier technique is essentially a two-field formulation. The Lagrange multipliers act directly as forces between contacting bodies.

Recently, several researchers have proposed methods which formulate the so-called intermediate contact surfaces, over which contact quantities can be defined and discretized. Examples of such ideas are to be found in References [8–10]. Further extensions of these approaches can

*Correspondence to: K. C. Park, Center for Aerospace Structures and Department of Aerospace Engineering Sciences, University of Colorado at Boulder, Campus Box 429, Boulder, CO 80309-0429, U.S.A.
†E-mail: kcpark@titan.colorado.edu

Contract/grant sponsor: Sandia National Laboratories; contract/grant number: ASCI AS-5666
Contract/grant sponsor: Lawrence Livermore National Laboratories; contract/grant number: ASCI level-II B347880

Received 24 December 2000
Revised 14 June 2001

be found in References [11–13] and in the mortar-like approaches in References [8, 14, 15], which enforce pressure continuity on the contact surface. Specifically, in order to circumvent overcontraining in the approaches of References [11–13], the pressure continuity is enforced at selected surface nodes and for the remaining nodes a kinematic gap continuity is enforced. Consequently, this leads in general to an unsymmetric formulation, with the task of choosing the number of pressure and kinematic constraints left to the user.

In the present paper, first, we introduce a contact frame that is akin to the intermediate contact surface with one distinct difference, that is, the contact frame is now endowed with its independent displacement degrees of freedom and its associated equilibrium equations. The equilibrium equations for the frame displacements on the contact frame turn out to be the contact condition. The frame equilibrium equation consists of the localized Lagrange multipliers that are assigned to each side of the contacting substructures. Consequently, the displacements of the two contacting substructural surfaces are related to the frame displacement, instead of relating themselves directly, leading to a localized kinematic contact condition which is the variational dual to the frame equilibrium equation. Hence, the task of satisfying the contact patch test [16, 17] is reduced to the nodal placement of the contact frame displacement. Second, because the contact equilibrium condition and the contact kinematic condition are dual, one may express them into a variational functional. This leads to a symmetric solution matrix. Third, the locations and the number of the frame nodal points are uniquely determined as will be shown in Section 7. This means both the contact equilibrium equation on the contact frame and its dual kinematic condition are uniquely determined, thus leading to non-singular contact constraints.

In passing we mention that the present approach is essentially an extension of the variational framework presented by Park and Felippa [18, 19]. Specializations derived from this variational framework include: a direct flexibility method and its dual form for parallel computation [20], and an algorithm for extracting substructural flexibility from measured global flexibility [21]. It should also be noted that Aminpour *et al.* [22] presented an algorithm for interfacing non-matching grids by utilizing a similar variational approach as utilized in the present paper. A closer examination of their numerical examples, however, reveals that the interface construction procedures they employed apparently do not necessarily pass the patch test.

The contents of this paper are as follows. First, we introduce terminology and notational conventions. Then, we describe the contact frame that is placed in between two contacting surfaces. An expression for the virtual work of the contact tractions is derived that will be helpful for identifying the role of the localized Lagrange multipliers. Next, the two stages of contact computations are discussed, namely, the contact detection state (stage 1) and the stage in which the predicted contacting surfaces will slide and deform towards equilibrium within a load step (stage 2). This is followed by an in-depth derivation of the contact part of the first variation, which accounts for the tangential motion of the contact frame.

In the remaining part of this paper we specialize the general 3D-formulation to the case of 2D-contact. We first discuss the discretization of the 2D contact frame. A crucial ingredient in the formulation of the discrete contact frame is its node placement. We will accomplish the contact frame node placement by satisfying contact patch tests. For a piecewise linear contact frame and using collocated contact forces, we will show that we need to place the frame nodes at roots of the moment line to pass these tests. Next, we discuss the non-singularity of the formulation. Then, we discuss a slip discretization that uniquely defines the tangential

motion of the frame. Discrete first and second variations are also presented. The latter shows the symmetry of our approach. We finish by presenting numerical results.

2. NOTATION

Two bodies that come in contact are depicted in Figure 1. All quantities related to body 1 will be denoted by non-barred quantities and the quantities related to body 2 will be denoted by barred quantities. Although the figure shows two contacting bodies, the picture is intended to capture also the case that two parts of the same body come in contact. Self-contact is therefore also implied. One should replace the terminology 'body' by 'contact side' for such cases.

The notation of the various quantities is based on the following conventions. Scalars are given in italics (e.g. a, A). Vectors and tensors are in bold-face (e.g. $\mathbf{a}, \boldsymbol{\alpha}$). Repeated tensor and matrix indices appearing as *both* subindex and superindex, as in

$$a_i b^i, \quad a_i b^i c_i, \quad A_i^i$$

imply summation. Repeated indices that appear only as subindex or superindex, as in

$$a_i b_i, \quad a^i b^i c^i, \quad A_{ii}$$

do *not* imply summation. The usual convention that Latin indices run from 1 to 3 and Greek indices run from 1 to 2 will be adopted.

3. CONTACT FRAME

The contact system of Figure 1 is redrawn in Figure 2 by separating the two contacting bodies in opposite directions. A contact frame is placed at the original contact position. The vertical dashed lines indicate corresponding points on the bodies and the contact frame. That is, the points connected by the vertical dashed lines have identical positions in space.

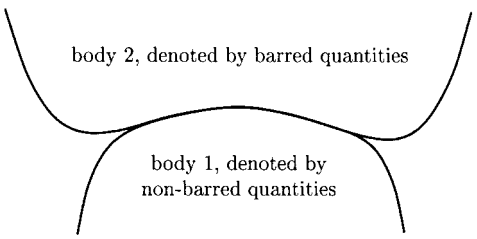

Figure 1. Contact between two bodies.

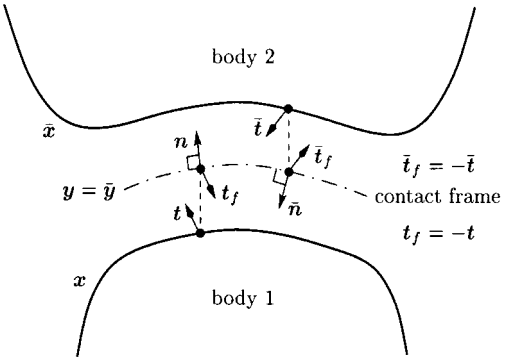

Figure 2. Expanded view of contact between two bodies with a contact frame placed in between.

The contact frame is introduced as a new element in the description of contact problems. Each body contacts one of its sides and exerts forces on the frame. The total force system on the contact frame is then required to be in self-equilibrium. This property is expected to produce high accuracy in the computed contact forces. The contact frame can be seen as a transducer that transfers the action of one body onto the other in a way that satisfies momentum balance.

The motion of body 1 is described by a displacement $\mathbf{u}$ from its reference position $\mathbf{X}$. The motion of body 2 is described by a displacement $\bar{\mathbf{u}}$ from its reference position $\bar{\mathbf{X}}$. The current positions $\mathbf{x}$ and $\bar{\mathbf{x}}$ of bodies 1 and 2, respectively, are thus given by

$$\mathbf{x} = \mathbf{X} + \mathbf{u}, \quad \bar{\mathbf{x}} = \bar{\mathbf{X}} + \bar{\mathbf{u}} \tag{1}$$

and are indicated in Figure 2.

The description of the motion of the contact frame should include the rigid body motions. Moreover, it should be able to deform so that the bodies on either side can deform during contact. The position $\mathbf{y}$ of the contact frame is composed of a reference position $\mathbf{Y}$ and a relative displacement $\mathbf{v}$ such that

$$\mathbf{y} = \mathbf{Y} + \mathbf{v} \tag{2}$$

We choose the reference position $\mathbf{Y}$ to be the *current* position of the contact frame. We also introduce the notation $\bar{\mathbf{y}}$ for the description of the position of the contact frame from the opposing side. By definition, we set $\bar{\mathbf{y}}$ equal to $\mathbf{y}$ and we have

$$\bar{\mathbf{y}} = \bar{\mathbf{Y}} + \bar{\mathbf{v}} \quad \text{with } \bar{\mathbf{Y}} = \mathbf{Y} \quad \text{and} \quad \bar{\mathbf{v}} = \mathbf{v} \tag{3}$$

Thus, we use $\mathbf{y}$ to describe the contact frame side where body 1 contacts and use $\bar{\mathbf{y}}$ to describe the contact frame side where body 2 contacts. This makes it possible to use similar notations for the description of the contact on either side of the contact frame. Also, it allows different descriptions of the *same* contact frame depending on the side of contact. This will prove to be convenient.

4. VIRTUAL WORK OF CONTACT TRACTIONS

The tractions acting on the contacting bodies are drawn in the expanded view of Figure 2. Momentum balance requires that the tractions acting on the contact frame are equal in magnitude and opposite in sign to the tractions acting on the corresponding points of the contacting bodies. The virtual work of the contact tractions is given by

$$\begin{aligned} \delta W_{\mathrm{c}} &= \int\!\!\int_{\mathscr{A}_{\mathrm{c}}} (\mathbf{t} \cdot \delta\mathbf{u} + \mathbf{t}_f \cdot \delta\mathbf{v})\, \mathrm{d}\mathscr{A} + \int\!\!\int_{\bar{\mathscr{A}}_{\mathrm{c}}} (\bar{\mathbf{t}} \cdot \delta\bar{\mathbf{u}} + \bar{\mathbf{t}}_f \cdot \delta\bar{\mathbf{v}})\, \mathrm{d}\bar{\mathscr{A}} \\ &= \int\!\!\int_{\mathscr{A}_{\mathrm{c}}} \mathbf{t} \cdot (\delta\mathbf{u} - \delta\mathbf{v})\, \mathrm{d}\mathscr{A} + \int\!\!\int_{\bar{\mathscr{A}}_{\mathrm{c}}} \bar{\mathbf{t}} \cdot (\delta\bar{\mathbf{u}} - \delta\bar{\mathbf{v}})\, \mathrm{d}\bar{\mathscr{A}} \quad \text{with } \delta\mathbf{v} = \delta\bar{\mathbf{v}} \end{aligned} \tag{4}$$

The notations $\mathscr{A}_{\mathrm{c}}$ and $\bar{\mathscr{A}}_{\mathrm{c}}$ are used to indicate the contact areas of bodies 1 and 2, respectively. In the continuum description these are identical, whereas they can be different when the contact

system is discretized. Similarly, $\mathrm{d}\mathscr{A}$ and $\mathrm{d}\bar{\mathscr{A}}$ represent infinitesimal contact areas of bodies 1 and 2, respectively. All areas refer to the *current* configuration of the bodies.

The contact tractions are now decomposed into normal and tangential components. To this end, we introduce a locally orthonormal base system $\mathbf{a}_i$ at each contact frame point such that $\mathbf{a}_3$ is normal to the contact frame. On the opposing side of the contact frame define $\bar{\mathbf{a}}_i = -\mathbf{a}_i$. Finally, introduce the special notation $\mathbf{n} = \mathbf{a}_3$ and $\bar{\mathbf{n}} = \bar{\mathbf{a}}_3$ for the normals. The decomposition of the contact tractions into normal and tangential components becomes

$$\mathbf{t}_f = -\mathbf{t} = \lambda^i \mathbf{a}_i, \quad \bar{\mathbf{t}}_f = -\bar{\mathbf{t}} = \bar{\lambda}^i \bar{\mathbf{a}}_i \tag{5}$$

The special notation $\lambda = \lambda^3$ and $\bar{\lambda} = \bar{\lambda}^3$ is introduced for the normal components of the contact tractions. Finally, the orientation of the normals $\mathbf{n}$ and $\bar{\mathbf{n}}$ is chosen such that both λ and $\bar{\lambda}$ will be positive in compression. This choice of orientation for the normals is illustrated in Figure 2. The choice for base system $\bar{\mathbf{a}}_i$ is motivated by the fact that it makes $\lambda^i = \bar{\lambda}^i$ in the continuum description as a result of momentum balance.

Substitution of the expressions for $\mathbf{t}$ and $\bar{\mathbf{t}}$ into the virtual work of the contact forces yields

$$\delta W_{\mathrm{c}} = -\int\!\!\int_{\mathscr{A}_{\mathrm{c}}} (\lambda \mathbf{n} + \lambda^\alpha \mathbf{a}_\alpha) \cdot (\delta \mathbf{u} - \delta \mathbf{v})\, \mathrm{d}\mathscr{A} - \int\!\!\int_{\bar{\mathscr{A}}_{\mathrm{c}}} (\bar{\lambda} \bar{\mathbf{n}} + \bar{\lambda}^\alpha \bar{\mathbf{a}}_\alpha) \cdot (\delta \bar{\mathbf{u}} - \delta \bar{\mathbf{v}})\, \mathrm{d}\bar{\mathscr{A}} \tag{6}$$

This expression will be useful to identify the Lagrange multipliers, which will be introduced later, with the components of the contact tractions.

5. CONTACT ENFORCEMENT

Consider two bodies that come in contact. Select from the contact zone of one body an arbitrary point, which we call the hitting point, and consider the contact of this point with the target surface of the other body. This situation is depicted in Figure 3. The configuration of the target surface at three different moments in time is distinguished by $\{\mathrm{A}, \mathrm{B}, \mathrm{C}\}$. The location of the hitting point at the same three moments in time is indicated by $\{\mathrm{A}', \mathrm{B}', \mathrm{C}'\}$. Positions A and A′ are before contact, position B and B′ are at the instant of *first* contact and positions C and C′ are after the instant of first contact.

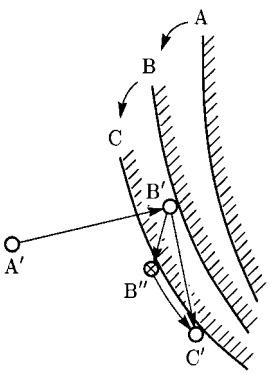

Figure 3. Motion of hitting node and target surface.

Looking at the computation of contact, similar stages can be recognized. If contact occurs within a load (or time) step, the positions B and B′ then correspond to the *predicted* contact location. The position A and A′ become the configuration from which the step is taken. At the end of the step, all forces are in equilibrium at positions C and C′. This leads us to the following subdivision of computational stages:

Stage 1: *Detection of contact* (*prediction*). The contact between a (hitting) point and the (target) surface it hits has to be detected.

Stage 2: *Sliding and deforming towards equilibrium* (*correction*). A detected contact from stage 1 only *predicts* the contact location. The hitting point will slide along its moving (and deforming) target surface starting at its predicted location until force equilibrium is established within the bounds of the surface characteristics.

The detection of contact involves the motion of the target surface from A to B and the motion of the hitting point from A′ to B′. Sliding and deforming towards equilibrium involves the motion of the target surface from B to C and the motion of the hitting point from B′ to C′. Essentially, this scheme is recognized as a predictor–corrector algorithm with the first stage as predictor and the second as corrector.

The first stage is known as contact search. Many contact search algorithms can be found in the literature. Hierarchical contact search [5, 23, 24] and bucket search [5, 25, 26] can be mentioned. When a point is already in contact with a hitting surface in the previous step, the contact search is not needed. The contact location in the previous step can then be taken as the prediction for the next step.

The second stage includes the solution of a set of non-linear contact constraint equations. This takes into account the effect that contact will have on the motion of the bodies (including deformations) as well as the change in contact location. This is represented in Figure 3 by the motion from B′ to B″ without a change in contact location plus a slide from B″ to the final position in C′. The sliding motion accounts for the fact that the magnitude of the frictional forces cannot exceed the maximum frictional force that can be generated on the contact surface.

The introduction of the contact frame in contact computations affects the formulation of the second stage. Therefore, in the following this stage is considered in detail. Detailed descriptions of the first stage can be found in the literature and are not given here.

6. VARIATIONAL FORMULATION OF A FRAME-BASED CONTACT MODEL

The contact part of the first variation should be set-up to define the motion of the contact frame. Traditional contact formulations do not have this requirement since the contact frame is then absent. The definition of the motion of the contact frame in its normal direction (normal motion) is dictated by the normal motions of the contacting bodies. Therefore, defining this motion poses no problems. However, the motion of the contact frame tangential to its own plane (tangential motion) needs careful consideration. Even for a frictionless formulation, we still need to define the tangential motion since the frame nodes can move tangentially.

In the case of frictional contact, the local conditions on the contact surface prescribe whether a state of stick (resp. slip), where the relative velocity is zero (resp. non-zero), will persist. Basically, we follow the approach advocated in Reference [13] to implement these two states.

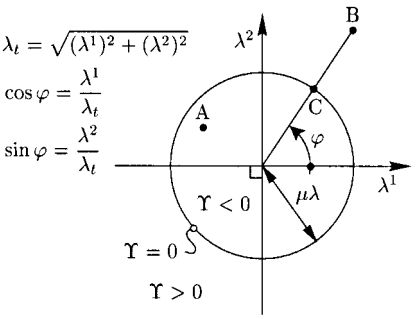

Figure 4. Friction yield function.

A constitutive framework is needed to discern the two states and transitions between them. To this end, define a single yield function

$$\Upsilon = \sqrt{(\lambda^1)^2 + (\lambda^2)^2} - \mu\lambda \tag{7}$$

in which μ represents the Coulomb friction coefficient. On the opposing side of the contact frame a similar yield function $\bar{\Upsilon}$ is defined. However, since the surface characteristics are the same on both sides of the contact frame we have $\mu = \bar{\mu}$. The yield function is required to be negative or zero. A negative value $\Upsilon < 0$ represents a state of stick, while slip will be incipient for $\Upsilon = 0$. Hence, the traction $\lambda^\alpha \mathbf{a}_\alpha$ has to remain inside ($\Upsilon < 0$) or on ($\Upsilon = 0$), a circular yield surface $\Upsilon = 0$ with radius $\mu\lambda$ (see Figure 4).

The gap normal to the contact surface has to remain zero on the contact surface. Mathematically, this can be written as

$$\begin{aligned} &\mathbf{x} - \mathbf{y} = \boldsymbol{\kappa} \quad \text{with } \boldsymbol{\kappa} = \kappa^\alpha \mathbf{a}_\alpha = \kappa_\alpha \mathbf{a}^\alpha \quad (\mathbf{a}_\alpha = \mathbf{a}^\alpha \text{ and } \kappa_\alpha = \kappa^\alpha) \\ &\bar{\mathbf{x}} - \bar{\mathbf{y}} = \bar{\boldsymbol{\kappa}} \quad \text{with } \bar{\boldsymbol{\kappa}} = \bar{\kappa}^\alpha \bar{\mathbf{a}}_\alpha = \bar{\kappa}_\alpha \bar{\mathbf{a}}^\alpha \quad (\bar{\mathbf{a}}_\alpha = \bar{\mathbf{a}}^\alpha \text{ and } \bar{\kappa}_\alpha = \bar{\kappa}^\alpha) \end{aligned} \tag{8}$$

This equation allows slip displacements $\boldsymbol{\kappa}$ and $\bar{\boldsymbol{\kappa}}$ tangent to the contact frame. These slip displacements cannot be independent since that would leave the tangential motion of the contact frame undefined. To deal with this, we set

$$\kappa_\alpha = \bar{\kappa}_\alpha \tag{9}$$

which defines the tangential motion of the frame to be the *average* of the tangential motion of the two bodies on either side of the contact surface. The gap constraints (8) are decomposed into normal and tangential directions and enforced in a weak sense using the variational form

$$\begin{aligned} \delta\pi_c^{\text{total}} = &\int\!\!\int_{\mathscr{A}_c} (\delta\{\lambda \mathbf{n}\cdot(\mathbf{x}-\mathbf{y})\} + \delta\{\lambda^\alpha \mathbf{a}_\alpha \cdot (\mathbf{x}-\mathbf{y})\} + \delta\{\gamma\kappa_\alpha(\lambda_l^\alpha - \lambda^\alpha) + \tfrac{1}{2}(1-\gamma)\kappa_\alpha\kappa^\alpha\})\,\mathrm{d}\mathscr{A} \\ &+ \int\!\!\int_{\bar{\mathscr{A}}_c} (\delta\{\bar{\lambda}\bar{\mathbf{n}}\cdot(\bar{\mathbf{x}}-\bar{\mathbf{y}})\} + \delta\{\bar{\lambda}^\alpha \bar{\mathbf{a}}_\alpha \cdot (\bar{\mathbf{x}}-\bar{\mathbf{y}})\} + \delta\{\bar{\gamma}\bar{\kappa}_\alpha(\bar{\lambda}_l^\alpha - \bar{\lambda}^\alpha) + \tfrac{1}{2}(1-\bar{\gamma})\bar{\kappa}_\alpha\bar{\kappa}^\alpha\})\,\mathrm{d}\bar{\mathscr{A}} \end{aligned} \tag{10}$$

To discuss this variational form let us investigate the integrand over $\mathscr{A}_c$, i.e. the contact between body 1 and the frame. We introduced the Lagrange multipliers λ, λ^α to enforce the

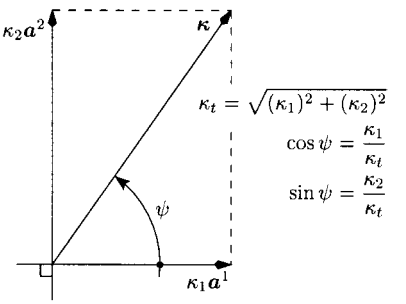

Figure 5. Direction of slip displacement.

gap constraint $\mathbf{x} - \mathbf{y} = \boldsymbol{\kappa}$ in normal and tangential directions. Comparing Equation (10) in its stick state, i.e. $\gamma = 0$ everywhere, with expression (6) for the virtual work of the contact tractions and setting $\delta\pi_c^{\text{total}} = -\delta W_c$ at equilibrium reveals that these Lagrange multipliers are the components of the contact tractions. The contact domain $\mathscr{A}_c$ is defined by the conditions

$$\mathbf{n} \cdot (\mathbf{x} - \mathbf{y}) = 0 \quad \text{where } \lambda \geqslant 0 \tag{11}$$

The third and fourth terms of the integrand govern the sliding behaviour of the model. Parameter γ is used as switch to either allow a point $\mathbf{x}$ to slide along the frame ($\gamma = 1$) or prohibit this sliding ($\gamma = 0$). This parameter is a function of position.

Two issues remain to be discussed, namely, when to switch between stick and slip states and how to define the constraint on the frictional force in the slip state. These issues are interconnected and resolved as follows. At the start of an analysis we have no knowledge about the appropriate state and assume the whole system is in a sticking state and set $\gamma = 0$ everywhere. This forces the slip displacement $\boldsymbol{\kappa}$ to be zero. Suppose that the resulting deformed configuration does not violate the yield condition, i.e. $\Upsilon \leqslant 0$ everywhere, so that no further action needs to be taken. Let all frictional tractions for this configuration be inside the yield surface (illustrated by point A in Figure 4). Increased loading will at some instant reach the transition state where $\Upsilon = 0$ and $\boldsymbol{\kappa} = 0$. This state still satisfies balance of linear momentum and the stick state is assumed to persist. Further loading finally violates the yield condition $\Upsilon \leqslant 0$ (illustrated by point B in Figure 4) and we need to switch to the slip state and have to set $\gamma = 1$ at such points. The direction of the frictional forces is defined by $\Upsilon = 0$ as being opposite to the direction of sliding. However, if the previous state was a sticking state, we have no previous sliding direction available and simply map the frictional force back to the yield surface in radial direction using (see point C in Figure 4)

$$\lambda_l^1 = \mu\lambda\cos\varphi, \quad \lambda_l^2 = \mu\lambda\sin\varphi \tag{12}$$

in which angle φ defines the direction of the frictional force in the previous iterate. When the previous state is a slipping state, a non-zero slipping direction is available. Therefore, we can set the constitutive equation that defines the frictional forces such that it is consistent with the yield condition $\Upsilon = 0$ and use (see Figure 5)

$$\lambda_l^1 = -\mu\lambda\cos\psi, \quad \lambda_l^2 = -\mu\lambda\sin\psi \tag{13}$$

in which angle ψ defines the direction of slip in the previous iterate. The convergence to the balance of linear momentum provides a direction of slip until the point of transition $\Upsilon = 0$ and $\boldsymbol{\kappa} = 0$ is reached again. Directional dependence of the frictional forces then becomes unavailable and we switch back to the stick state $\gamma = 0$. It is noted that the limiting values λ_l^α are set based on the previous iterate. We also note that the conditions used here to deal with the stick/slip states correspond precisely to those developed in Reference [27] for rigid plasticity. For the frictionless case, we can use $\mu = 0$ in our model and the difference between the constitutive definitions (12) and (13) vanishes.

In the remaining part of this section we first rewrite $\delta\pi_c^{\text{total}}$ in terms of the variational unknowns. The resulting expression is then used to illustrate that Equation (9) indeed defines the tangential motion of the frame to be the average of the tangential motion of the two contacting sides.

We begin by introducing two surface co-ordinates ξ^α that define the location of the contact point on the contact frame. The relation of these co-ordinates with the tangents $\mathbf{a}_\alpha$ is defined as

$$\mathbf{a}_\alpha = \frac{1}{\|\mathbf{y}_{,\alpha}\|}\mathbf{y}_{,\alpha}, \quad \text{where } (\,)_{,\alpha} = \frac{\partial(\,)}{\partial\xi^\alpha} \tag{14}$$

This definition implies that the ξ^α are orthogonal co-ordinates and its variation $\delta\xi^\alpha$ is *zero* in the present formulation.

In order to rewrite $\delta\pi_c^{\text{total}}$ in terms of the variational fields, $\delta\mathbf{a}_\alpha$ can be shown to be

$$\delta\mathbf{a}_\alpha = \mathbf{Q}_\alpha\delta\mathbf{v}_{,\alpha}, \quad \text{where } \mathbf{Q}_\alpha = \frac{1}{\|\mathbf{y}_{,\alpha}\|}(\mathbf{I} - \mathbf{a}_\alpha \otimes \mathbf{a}_\alpha) \tag{15}$$

Using this expression for $\delta\mathbf{a}_\alpha$ we find

$$\delta\{\mathbf{a}_\alpha \cdot (\mathbf{x} - \mathbf{y})\} = \mathbf{a}_\alpha \cdot (\delta\mathbf{u} - \delta\mathbf{v}) + [\mathbf{Q}_\alpha(\mathbf{x} - \mathbf{y})] \cdot \delta\mathbf{v}_{,\alpha} \tag{16}$$

Since the base system $\mathbf{a}_i$ is orthonormal, we can define the normal as $\mathbf{n} = \mathbf{a}_1 \times \mathbf{a}_2$ and find its variation to be

$$\mathbf{n} = \mathbf{a}_1 \times \mathbf{a}_2 \;\Rightarrow\; \delta\mathbf{n} = \mathrm{e}^{\beta\alpha}(\mathbf{a}_\beta \times \mathbf{I})\mathbf{Q}_\alpha\delta\mathbf{v}_{,\alpha} \tag{17}$$

where the orientation of $\mathbf{a}_1$ and $\mathbf{a}_2$ should be such that it defines the direction of the normal as indicated in Figure 2 and $\mathrm{e}^{\alpha\beta}$ represents the permutation symbol. Using this expression for $\delta\mathbf{n}$ we find

$$\delta\{\mathbf{n} \cdot (\mathbf{x} - \mathbf{y})\} = \mathbf{n} \cdot (\delta\mathbf{u} - \delta\mathbf{v}) + [\mathrm{e}^{\alpha\beta}\mathbf{Q}_\alpha(\mathbf{a}_\beta \times \mathbf{I})(\mathbf{x} - \mathbf{y})] \cdot \delta\mathbf{v}_{,\alpha} \tag{18}$$

Using these expressions one finds that $\delta\pi_c^{\text{total}}$ is given by

$$\delta\pi_c^{\text{total}} = \delta\pi_c + \delta\bar{\pi}_c \tag{19}$$

where

$$\delta\pi_c = \iint_{\mathscr{A}_c} (\delta\lambda\{\mathbf{n} \cdot (\mathbf{x} - \mathbf{y})\} + \delta\lambda^\alpha\{\mathbf{a}_\alpha \cdot (\mathbf{x} - \mathbf{y}) - \gamma\kappa_\alpha\} + \delta\mathbf{u} \cdot \{\lambda\mathbf{n} + \lambda^\alpha\mathbf{a}_\alpha\} - \delta\mathbf{v} \cdot \{\lambda\mathbf{n} + \lambda^\alpha\mathbf{a}_\alpha\}$$
$$+ \delta\mathbf{v}_{,\alpha} \cdot \{\mathbf{Q}_\alpha\boldsymbol{\Phi}^\alpha(\mathbf{x} - \mathbf{y})\} + \delta\kappa_\alpha\{\gamma(\lambda_l^\alpha - \lambda^\alpha) + (1 - \gamma)\kappa^\alpha\})\,\mathrm{d}\mathscr{A}$$

$$\delta\bar{\pi}_{\mathrm{c}} = \iint_{\bar{\mathscr{A}}_{\mathrm{c}}} (\delta\bar{\lambda}\{\bar{\mathbf{n}}\cdot(\bar{\mathbf{x}}-\bar{\mathbf{y}})\} + \delta\bar{\lambda}^{\alpha}\{\bar{\mathbf{a}}_{\alpha}\cdot(\bar{\mathbf{x}}-\bar{\mathbf{y}}) - \bar{\gamma}\bar{\kappa}_{\alpha}\} + \delta\bar{\mathbf{u}}\cdot\{\bar{\lambda}\bar{\mathbf{n}} + \bar{\lambda}^{\alpha}\bar{\mathbf{a}}_{\alpha}\} - \delta\bar{\mathbf{v}}\cdot\{\bar{\lambda}\bar{\mathbf{n}} + \bar{\lambda}^{\alpha}\bar{\mathbf{a}}_{\alpha}\}$$
$$+ \delta\bar{\mathbf{v}}_{,\bar{\alpha}}\cdot\{\bar{\mathbf{Q}}_{\alpha}\bar{\mathbf{\Phi}}^{\alpha}(\bar{\mathbf{x}}-\bar{\mathbf{y}})\} + \delta\bar{\kappa}_{\alpha}\{\bar{\gamma}(\bar{\lambda}_{l}^{\alpha} - \bar{\lambda}^{\alpha}) + (1-\bar{\gamma})\bar{\kappa}^{\alpha}\})\,\mathrm{d}\bar{\mathscr{A}}$$

in which we have introduced the definitions

$$\mathbf{\Phi}^{\alpha} = \lambda^{\alpha}\mathbf{I} + \lambda \mathrm{e}^{\alpha\beta}(\mathbf{a}_{\beta}\times\mathbf{I}), \quad \bar{\mathbf{\Phi}}^{\alpha} = \bar{\lambda}^{\alpha}\mathbf{I} - \bar{\lambda}\mathrm{e}^{\alpha\beta}(\bar{\mathbf{a}}_{\beta}\times\mathbf{I})$$

The equilibrium of two bodies that come in contact is described by adding $\delta\pi_{\mathrm{c}}^{\mathrm{total}}$ to the first variation of the two individual bodies and then require that the resulting first variation vanishes. This yields a non-linear set of equations.

The force equilibrium equation in the contact domain will be provided by the coefficients of $\delta\mathbf{v}$ (and $\delta\bar{\mathbf{v}}$, but $\delta\mathbf{v} = \delta\bar{\mathbf{v}}$). As mentioned earlier, the appearance of this equation is the result of the introduction of the contact frame with independent displacement freedoms. A second interesting point is that the integrations that have to be performed are kept strictly local to each side of the contact frame.

At this point we would like to draw attention to the differences between our frame-based formulation and other contact formulations. For this purpose it is instructive to write the first variation of the complete system, in the form

$$\delta\pi = \delta\pi_{\mathrm{free}}^{\mathrm{total}} + \delta\pi_{\mathrm{c}}^{\mathrm{total}} \tag{20}$$

where

$$\delta\pi_{\mathrm{free}}^{\mathrm{total}} = \delta\pi_{\mathrm{free}} + \delta\bar{\pi}_{\mathrm{free}}, \quad \delta\pi_{\mathrm{c}}^{\mathrm{total}} = \delta\pi_{\mathrm{c}} + \delta\bar{\pi}_{\mathrm{c}}$$
$$\delta\pi_{\mathrm{free}} = G, \quad \delta\pi_{\mathrm{c}} = G_{\mathrm{c}\lambda} - G_{\mathrm{c}u} + G_{\mathrm{c}\kappa} - G_{\mathrm{c}v}$$
$$\delta\bar{\pi}_{\mathrm{free}} = \bar{G}, \quad \delta\bar{\pi}_{\mathrm{c}} = \bar{G}_{\mathrm{c}\lambda} - \bar{G}_{\mathrm{c}u} + \bar{G}_{\mathrm{c}\kappa} - \bar{G}_{\mathrm{c}v}$$

in which $G(\mathbf{x};\delta\mathbf{u})$ and $\bar{G}(\bar{\mathbf{x}};\delta\bar{\mathbf{u}})$ are the first variations of the two bodies excluding contact, and the remaining expressions are given by

$$\begin{aligned}
G_{\mathrm{c}\lambda}(\mathbf{x},\mathbf{y},\kappa_{\alpha};\delta\lambda,\delta\lambda^{\alpha}) &= \iint_{\mathscr{A}_{\mathrm{c}}} (\delta\lambda\{\mathbf{n}\cdot(\mathbf{x}-\mathbf{y})\} + \delta\lambda^{\alpha}\{\mathbf{a}_{\alpha}\cdot(\mathbf{x}-\mathbf{y}) - \gamma\kappa_{\alpha}\})\,\mathrm{d}\mathscr{A} \\
G_{\mathrm{c}u}(\mathbf{y},\lambda,\lambda^{\alpha};\delta\mathbf{u}) &= \iint_{\mathscr{A}_{\mathrm{c}}} (-\delta\mathbf{u}\cdot\{\lambda\mathbf{n} + \lambda^{\alpha}\mathbf{a}_{\alpha}\})\,\mathrm{d}\mathscr{A} \\
G_{\mathrm{c}\kappa}(\mathbf{y},\lambda^{\alpha},\kappa^{\alpha};\delta\kappa_{\alpha}) &= \iint_{\mathscr{A}_{\mathrm{c}}} (\delta\kappa_{\alpha}\{\gamma(\lambda_{l}^{\alpha} - \lambda^{\alpha}) + (1-\gamma)\kappa^{\alpha}\})\,\mathrm{d}\mathscr{A} \\
G_{\mathrm{c}v}(\mathbf{x},\mathbf{y},\lambda,\lambda^{\alpha};\delta\mathbf{v}) &= \iint_{\mathscr{A}_{\mathrm{c}}} (\delta\mathbf{v}\cdot\{\lambda\mathbf{n} + \lambda^{\alpha}\mathbf{a}_{\alpha}\} - \delta\mathbf{v}_{,\alpha}\cdot\{\mathbf{Q}_{\alpha}\mathbf{\Phi}^{\alpha}(\mathbf{x}-\mathbf{y})\})\,\mathrm{d}\mathscr{A}
\end{aligned} \tag{21}$$

and similarly for the barred side. It should be noted that $G_{\mathrm{c}\lambda}(\mathbf{x},\mathbf{y},\kappa_{\alpha};\delta\lambda,\delta\lambda^{\alpha})$ constitutes the kinematic constraint between the contact surface $\mathbf{x}$ and contact frame $\mathbf{y}$, $G_{\mathrm{c}u}(\mathbf{y},\lambda,\lambda^{\alpha};\delta\mathbf{u})$ the virtual work of the contact traction acting on contact surface $\mathbf{x}$, $G_{\mathrm{c}\kappa}(\mathbf{y},\lambda^{\alpha},\kappa^{\alpha};\delta\kappa_{\alpha})$ the constraint on the frictional behaviour, and $G_{\mathrm{c}v}(\mathbf{x},\mathbf{y},\lambda,\lambda^{\alpha};\delta\mathbf{v})$ the virtual work of the contact traction acting

on contact frame $\mathbf{y}$, respectively. Similarly, the four corresponding terms in $\delta\bar{\pi}_c$ can also be identified.

Of particular importance in the present formulation is the equilibrium equation of the contact frame, which, among other terms, is obtained by setting the first variation $\delta\pi$ equal to zero:

$$G_{cv}(\mathbf{x}, \mathbf{y}, \lambda, \lambda^\alpha; \delta\mathbf{v}) + \bar{G}_{cv}(\bar{\mathbf{x}}, \bar{\mathbf{y}}, \bar{\lambda}, \bar{\lambda}^\alpha; \delta\bar{\mathbf{v}}) = 0 \tag{22}$$

This equation accounts for equilibrium conditions on the contact, viz., the traction continuity condition in the contact domain. In particular, this equation results since the contact frame surface is endowed with independent kinematic variables $\mathbf{v}$ (or $\bar{\mathbf{v}}$, but $\mathbf{v} = \bar{\mathbf{v}}$). As a result, the traction continuity condition $\mathbf{t} = -\bar{\mathbf{t}}$ (see Figure 2) is enforced in a weak sense in our formulation. It needs to be noted that the approach taken in References [11–13] also enforces traction continuity on the contact domain in a weak sense. However, in that approach continuity of traction components ($\lambda^i = \bar{\lambda}^i$) is enforced in a weak sense as opposed to enforcement of continuity of the traction vectors ($\mathbf{t} = -\bar{\mathbf{t}}$) in the present formulation. For the continuum case this makes no difference. However, discrete contact surfaces do not match in general. Discarding the direction of the contact tractions results for general discrete contact descriptions in violation of momentum balance.

We would like to point out that the approach taken by McDevitt and Laursen [8] does utilize the concept of an intermediate surface in between contacting bodies. They use the intermediate surface to define a common discretization for both sides and map the unknowns from either side on this shared discretization of the contact domain. Then, they can proceed by establishing node-to-node contact in the classical sense. An independent variable to describe the motion of their intermediate surface never enters the formulation and traction continuity on the contact domain has to be satisfied on the continuum level.

We now offer the following remarks regarding the present localized formulation:

1. Unlike the classical contact formulation, the localized contact tractions on each contact surface are treated as independent variables.
2. Unlike mortar or mortar-like approaches [8], the need for introducing mortar interpolation schemes is alleviated.
3. The present formulation enables the utilization of additional independent variables for enforcing contact conditions for both matching and non-matching discrete contact surfaces. This is accomplished by the pairs of localized Lagrange multipliers ($\lambda^i, \bar{\lambda}^i$), and the independent contact frame displacements $\mathbf{v}$ (or $\bar{\mathbf{v}}$, but $\mathbf{v} = \bar{\mathbf{v}}$).
4. The contact frame equilibrium equation (22) makes its possible to completely modularize the contact enforcement part, independent of the governing equations of the contacting structures.

Our formulation enforces traction continuity in the contact domain in a weak sense. This weak enforcement is consistent with the finite element discretization of structural problems. This feature of our formulation actually localizes the contact tractions and is the basis for each of the remarks stated above.

The coefficients of $(\delta\lambda, \delta\lambda^\alpha)$ and $(\delta\bar{\lambda}, \delta\bar{\lambda}^\alpha)$ in (19) define the frame position to be

$$\mathbf{x} - \mathbf{y} = \kappa_\alpha \mathbf{a}^\alpha \quad \text{and} \quad \bar{\mathbf{x}} - \bar{\mathbf{y}} = \bar{\kappa}_\alpha \bar{\mathbf{a}}^\alpha \tag{23}$$

in which we have set $\gamma = 1$ and $\bar{\gamma} = 1$ and thereby assume that the constraint on the frictional traction is active. Constraints (23) require the contacting points $\mathbf{x}$ and $\bar{\mathbf{x}}$ to remain on the

tangent plane to the contact surface at $\mathbf{y}$. Using $\bar{\mathbf{y}} = \mathbf{y}$, $\bar{\mathbf{a}}_\alpha = -\mathbf{a}_\alpha$ together with definition (9) yields in tangential direction

$$\mathbf{a}_\alpha \cdot \mathbf{y} = \tfrac{1}{2}\mathbf{a}_\alpha \cdot (\mathbf{x} + \bar{\mathbf{x}}) \quad \text{and} \quad \bar{\boldsymbol{\kappa}} = -\boldsymbol{\kappa} \tag{24}$$

This defines the tangential frame motion to be the *average* of the tangential motions of the two contacting sides.

After obtaining values for the κ_α, one can update the contact co-ordinates using

$$(\xi^\alpha)^{i+1} = (\xi^\alpha)^i + (\Delta\xi^\alpha)^i, \quad \text{where } \Delta\xi^\alpha = \frac{\kappa_\alpha}{\|\mathbf{y}_{,\alpha}\|} \tag{25}$$

in which i represents an iteration index. After this update, the κ_α are reset to zero so that the κ_α keep their interpretation of slip displacements within a slip iteration. The first variation defines the slip displacement κ_α to be zero when the constraint on the frictional force is not active, i.e. when $\gamma = 0$ then $\kappa_\alpha = 0$.

7. CONSTRUCTION OF DISCRETE CONTACT INTERFACES FOR 2D-CASE

The variational formulation of frame-based contact problems presented in Section 6 applies to the general 3D-case. In the rest of the present paper we will focus on 2D problems primarily to render the role of the contact frame as succinctly as possible to the reader. To this end, let $\{\mathbf{E}_1, \mathbf{E}_2, \mathbf{E}_3\}$ be the unit triad and let the 2D contact take place in the plane spanned by $\{\mathbf{E}_2, \mathbf{E}_3\}$. We select the two tangent vectors $\mathbf{a}_2$ and $\bar{\mathbf{a}}_2$ to follow the contact frame line in the $\{\mathbf{E}_2, \mathbf{E}_3\}$ plane. Furthermore, we set

$$\mathbf{a}_1 = \mathbf{E}_1, \quad \bar{\mathbf{a}}_1 = -\mathbf{E}_1 \tag{26}$$

With these geometrical parametrizations, we now detail the discretization of the frame and the frame node determination.

Up to this point the formulation applies to the continuum formulation. However, we have introduced the concept of a contact frame with application to the finite element method in mind. Therefore, the next question is how to discretize our contact frame. As a key objective of the present study, we would like to obtain a generic discrete contact frame, as illustrated in Figure 6, that should not depend on specific element formulations used to discretize the contacting bodies. Therefore, it should use only nodal information from the contacting bodies. In other words, as far as the frame is concerned, the bodies can be replaced by a set of collocated forces touching the contact frame at distinct places. Ideally, such a generic contact interface can be applied to any contact problem without tailoring it to the specifics of the FEM models of the bodies in contact. We regard this as the key advantage of our formulation that justifies the introduction of additional unknowns, namely, the localised Lagrange multipliers that usually double the number of classical Lagrange multipliers and the frame displacement $\mathbf{v}$ introduced in (2).

The contact frame is described by a collection of linearly interpolated segments in between contact frame nodes. The exploded view of Figure 6 shows such a contact frame. The dash–dot lines are the linear contact frame segments that run in between the contact frame nodes (open dots). The filled dots represent the discretization of the contacting bodies on their boundaries. The interpolation used over the boundaries of the contacting bodies is not so restricted.

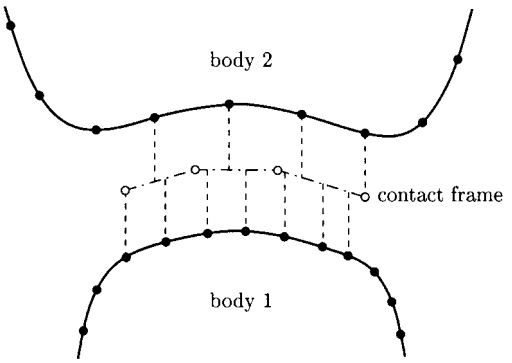

Figure 6. Contact frame discretization.

To obtain the contact frame position, we do a contact search. Basically, this establishes a list of boundary segments that come into contact with a node of the boundary of the body on the opposing side of the contact frame. Putting all the nodes connected to these segments in sequence results in a description of the location of the contact frame. One obtains such a sequence of nodes in Figure 6 by closing the expanded view in vertical direction.

The two meshes in the contact zone of the bodies on either side of the contact frame are inherently non-matching. Therefore, it is by no means trivial to come up with a contact frame mesh. Basically, three questions need to be answered. Firstly, how many frame position nodes should be used to define the contact frame? Secondly, where should these nodes be placed? Thirdly, how should the slip displacement field be discretized? The first two questions deal with the successful application of our approach in so called contact patch test conditions [16, 17]. The third question is about choosing a discrete definition of the tangential frame motion that is non-singular. The answers to all three questions determine whether the system of equations can be solved, i.e., is non-singular. This is related to satisfying the essential requirements of the Babuška–Brezzi [28, 29] conditions. We will now address each of these issues in separate subsections.

7.1. Frame nodal placement procedure

The design of any new method in computational mechanics must face a deceptively simple question, namely: 'How well can it represent constant stress states?' For example, a new finite element should survive a constant stress patch test in order to be able to claim that convergence to the correct result is expected when mesh refinement is applied. We intend to design our contact interface such that it will produce the correct results for constant stress states. The placement of the contact frame nodes plays a vital role in achieving this goal.

A typical patch test for testing the transfer of constant stress states between two bodies in contact is shown in Figure 7. The two bodies are loaded by a normal line load q acting at their free upper and lower boundaries. A key feature of a contact patch test is that the meshing of the contacting bodies is non-matching in the contact domain. It is standard procedure in finite element analysis to represent a constant line load by using energy equivalent forces applied at nodal points. Differences in boundary interpolation order manifest themselves in different values for these energy equivalent forces. The exploded view of Figure 7(b) shows

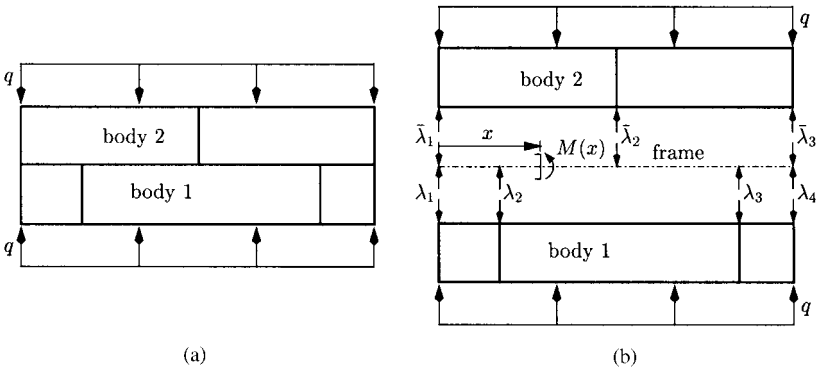

Figure 7. (a) Patch test example for contact between two bodies; and (b) exploded view showing the (collocated) energy equivalent forces $(\lambda_p, \bar{\lambda}_p)$ acting between the bodies and the frame.

the location of the energy equivalent forces λ_p and $\bar{\lambda}_p$ that represent the constant line load q in the contact domain. The set of these collocated forces will be referred to as the set of *patch test passing forces*. These forces are acting on the contact frame and equilibrium of the frame is governed by Equation (22). Linearization of the discrete version of this equation at the reference configuration leads to (see (42), (45) and (47) for details)

$$-[\mathbf{L}_b^{\mathrm{t}} \;\; \bar{\mathbf{L}}_b^{\mathrm{t}}] \begin{bmatrix} \boldsymbol{\lambda} \\ \bar{\boldsymbol{\lambda}} \end{bmatrix} = \mathbf{0} \quad \text{with } \boldsymbol{\lambda}^{\mathrm{t}} = [\lambda_1 \;\; \lambda_1^2 \;\; \ldots \;\; \lambda_P \;\; \lambda_P^2] \quad \text{and} \quad \bar{\boldsymbol{\lambda}}^{\mathrm{t}} = [\bar{\lambda}_1 \;\; \bar{\lambda}_1^2 \;\; \ldots \;\; \bar{\lambda}_{\bar{P}} \;\; \bar{\lambda}_{\bar{P}}^2] \tag{27}$$

in which (λ_p, λ_p^2) are the collocated normal and tangential forces acting on the frame at body nodes of body 1 and similarly we have forces $(\bar{\lambda}_p, \bar{\lambda}_p^2)$ acting on the frame at body nodes of body 2. The detailed derivation of this equation will be discussed in a separate section. In that section, we will show also that the linearization of the gap constraint equations at the reference configuration leads to (if the slip displacements are assumed to be zero)

$$\begin{bmatrix} \mathbf{B}^{\mathrm{t}} & \mathbf{0} \\ \mathbf{0} & \bar{\mathbf{B}}^{\mathrm{t}} \end{bmatrix} \begin{bmatrix} \mathbf{u} \\ \bar{\mathbf{u}} \end{bmatrix} - \begin{bmatrix} \mathbf{L}_b \\ \bar{\mathbf{L}}_b \end{bmatrix} \mathbf{v} = - \begin{bmatrix} \mathbf{g} \\ \bar{\mathbf{g}} \end{bmatrix} \tag{28}$$

in which $\mathbf{v}, \mathbf{u}$ and $\bar{\mathbf{u}}$ are the collection of discrete displacement vectors at all nodes of the frame, bodies 1 and 2, respectively. The boolean matrices $\mathbf{B}^{\mathrm{t}}$ and $\bar{\mathbf{B}}^{\mathrm{t}}$ serve to select the body nodes that are in the contact domain for bodies 1 and 2, respectively. The symmetry of our formulation manifests itself from the fact that the transpose of the $[\mathbf{L}_b^{\mathrm{t}} \;\; \bar{\mathbf{L}}_b^{\mathrm{t}}]$ matrix in Equation (27) also governs the compatibility between the body and frame displacements in Equation (28). In order to pass the contact patch test we need to ensure that the set of discrete contact patch test passing forces is a solution of frame equilibrium equation (27). We now offer the following proposition how this is achieved by the present frame node placement procedure (see References [30, 31] for the related application of this procedure to the problem of interfacing non-matching finite element meshes)

Proposition (*Zero moment rule*)
Let the moment $M(x)$ along a straight frame line be given by (see Figure 7 for an illustration)

$$M(x) = \sum_{p=1}^{P} \lambda_p \chi_p(x) - \sum_{p=1}^{\bar{P}} \bar{\lambda}_p \bar{\chi}_p(x) \tag{29}$$

where λ_p is the collocated patch test passing force at co-ordinate x_p on the non-barred side, $\bar{\lambda}_p$ the collocated patch test passing force at co-ordinate $\bar{x}_p$ on the barred side, P the total number of collocated patch test passing forces λ_p on the non-barred side, $\bar{P}$ the total number of collocated patch test passing forces $\bar{\lambda}_p$ on the barred side,

$$\chi_p(x) = \begin{cases} x - x_p & \text{if } x \geqslant x_p \\ 0 & \text{if } x < x_p \end{cases} \quad \text{and} \quad \bar{\chi}_p(x) = \begin{cases} x - \bar{x}_p & \text{if } x \geqslant \bar{x}_p \\ 0 & \text{if } x < \bar{x}_p \end{cases}$$

The forces $(\lambda_p, \bar{\lambda}_p)$, that define the moment $M(x)$ in Equation (29), are a set of *patch test passing forces*. They are obtained by first assuming a constant normal stress in the contacting bodies and then computing the corresponding energy equivalent forces $(\lambda_p, \bar{\lambda}_p)$ at body nodes of the contacting boundaries. In order for our frame-based formulation to pass the contact patch test, the frame nodes have to be placed at the $S+1$ roots of $M(x) = 0$, i.e. each frame node location x_s satisfies

$$M(x_s) = 0 \quad s = 1, \ldots, S+1 \tag{30}$$

with linearly interpolated frame segments between these zero moment points. This frame construction ensures the exact transfer of both constant normal and constant tangential line loads through the frame.

Proof
To prove this proposition we need to look at the behaviour of the discrete frame equilibrium equation (27). The form of the $[\mathbf{L}_b^{\mathrm{t}} \ \bar{\mathbf{L}}_b^{\mathrm{t}}]$ matrix determines whether the patch test passing set of forces is a solution of this equation. In this proof we will investigate the structure of the $[\mathbf{L}_b^{\mathrm{t}} \ \bar{\mathbf{L}}_b^{\mathrm{t}}]$ matrix in relation to the frame node placement.

We start by assuming that the contact frame is a straight line. Further, we set $\mathbf{v} = v\mathbf{n} + v^2\mathbf{a}_2$ and $\bar{\mathbf{v}} = \bar{v}\mathbf{n} + \bar{v}^2\mathbf{a}_2$, use $\bar{\mathbf{a}}_i = -\mathbf{a}_i$, and take a closed gap ($\mathbf{x} - \mathbf{y} = \mathbf{0}$) everywhere. Further, we localize each frame segment by cutting the frame at inner node points as shown at the left segment node in Figure 8. The displacement compatibility at the cuts is enforced by Lagrange multipliers R_s and R_s^2. Then, Equation (22) can be specialized for this case as

$$\sum_{s=1}^{S} \int_{\mathscr{A}_s} \{\lambda \delta v + \lambda^2 \delta v^2 - \bar{\lambda} \delta \bar{v} - \bar{\lambda}^2 \delta \bar{v}^2\} \, \mathrm{d}x + \sum_{s=2}^{S} \{\delta \{R_s (v_1^{(s)} - v_2^{(s-1)}) + R_s^2 (v_1^{2(s)} - v_2^{2(s-1)})\}\} = 0 \tag{31}$$

in which we used x to represent the co-ordinate length along the frame line. The frame is discretized using piecewise linear segments. Further, $\mathbf{v}$ and $\bar{\mathbf{v}}$ are merely different descriptions of the same displacement, i.e. we must have $\mathbf{v} = \bar{\mathbf{v}}$. Therefore, we represent the displacements on each segment by

$$\begin{aligned} v &= N_1 v_1^{(s)} + N_2 v_2^{(s)}, \quad v^{2(s)} = N_1 v_1^{2(s)} + N_2 v_2^{2(s)}, \quad N_1 = \tfrac{1}{2}(1-\xi), \quad N_2 = \tfrac{1}{2}(1+\xi) \\ \bar{v} &= \bar{N}_2 v_1^{(s)} + \bar{N}_1 v_2^{(s)}, \quad \bar{v}^{2(s)} = \bar{N}_2 v_1^{2(s)} + \bar{N}_1 v_2^{2(s)}, \quad \bar{N}_2 = \tfrac{1}{2}(1+\bar{\xi}), \quad \bar{N}_1 = \tfrac{1}{2}(1-\bar{\xi}) \end{aligned} \tag{32}$$

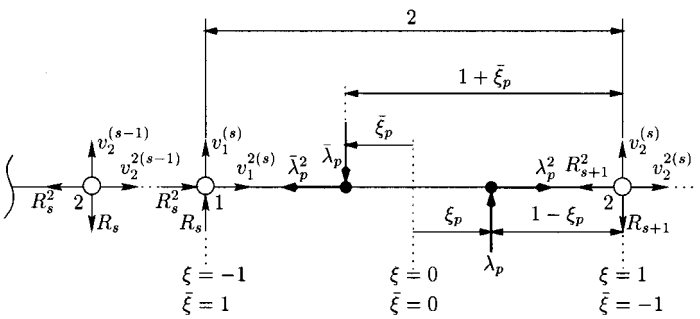

Figure 8. Contact frame segment s with collocated forces $\lambda_p\mathbf{n}+\lambda_p^2\mathbf{a}_2$ $(p=1,\ldots,P_s)$ and $\bar{\lambda}_p\bar{\mathbf{n}}+\bar{\lambda}_p^2\bar{\mathbf{a}}_2$ $(p=1,\ldots,\bar{P}_s)$ acting onto the frame segment from opposing sides. Lagrange multipliers R_s and R_s^2 serve to connect segment s on its left side to segment $s-1$.

in which ξ and $\bar{\xi}$ represent natural co-ordinates on the segment (see Figure 8 in which open dots represent frame nodes). The frame interacts with the bodies through a set of collocated forces at the nodal points of the contacting bodies. Mathematically, this can be represented by introducing a Dirac delta function δ (see Equation (39)). The components of the traction acting on a frame segment from body 1 are now defined by

$$\begin{bmatrix}\lambda(x)\\ \lambda^2(x)\end{bmatrix}=\sum_{p=1}^{P_s}\begin{bmatrix}\lambda_p(x)\\ \lambda_p^2(x)\end{bmatrix}\quad\text{where }\lambda_p(x)=\lambda_p\delta(x-x_p)\quad\text{and}\quad\lambda_p^2(x)=\lambda_p^2\delta(x-x_p)\tag{33}$$

in which $\lambda_p\mathbf{n}+\lambda_p^2\mathbf{a}_2$ is the collocated force acting on the frame at body node p of body 1 and P_s represents the total number of body nodes contacting segment s on the non-barred side. The tractions on the barred side are similarly defined. The collocated forces $\lambda_p\mathbf{n}+\lambda_p^2\mathbf{a}_2$ and $\bar{\lambda}_p\bar{\mathbf{n}}+\bar{\lambda}_p^2\bar{\mathbf{a}}_2$ act on the frame at co-ordinates ξ_p and $\bar{\xi}_p$, respectively, as illustrated in Figure 8. The filled dots in this figure merely indicate the point of application of these forces and do *not* represent frame nodes. Substituting (32) and (33) into Equation (31) we arrive, after some manipulations, at

$$\begin{aligned}&\left\{\sum_{p=1}^{P}\lambda_p(1-\xi_p)-\sum_{p=1}^{\bar{P}}\bar{\lambda}_p(1+\bar{\xi}_p)\right\}_s+2R_s=0\quad\text{for } s=1,\ldots,S\\ &\left\{\sum_{p=1}^{P}\lambda_p^2(1-\xi_p)-\sum_{p=1}^{\bar{P}}\bar{\lambda}_p^2(1+\bar{\xi}_p)\right\}_s+2R_s^2=0\quad\text{for } s=1,\ldots,S\end{aligned}\tag{34}$$

$$R_{S+1}=0\quad\text{(global normal force equilibrium)}$$

$$R_{S+1}^2=0\quad\text{(global tangential force equilibrium)}$$

in which the Lagrange multipliers R_s and R_s^2 are given by

$$\begin{bmatrix}R_1\\ R_1^2\end{bmatrix}=\mathbf{0}\quad\text{and}\quad\begin{bmatrix}R_s\\ R_s^2\end{bmatrix}=\sum_{r=1}^{s-1}\left\{\sum_{p=1}^{P_r}\begin{bmatrix}\lambda_p\\ \lambda_p^2\end{bmatrix}-\sum_{p=1}^{\bar{P}_r}\begin{bmatrix}\bar{\lambda}_p\\ \bar{\lambda}_p^2\end{bmatrix}\right\}\quad\text{for: } s=2,\ldots,S+1\tag{35}$$

The Lagrange multipliers R_s and R_s^2 take the role of applied forces needed to enforce displacement continuity. We note that R_1, R_1^2, R_{S+1} and R_{S+1}^2 are all zero since they represent the resultant forces at the (free) end points of the frame. Equations $(34)_{1-4}$ are now in the form (27) and they define the $2S+2$ rows of the $[\mathbf{L}_b^t\ \bar{\mathbf{L}}_b^t]$ matrix. We now arrive at a very important observation, namely, the discrete frame equilibrium equations $(34)_{1,2}$ will yield a force distribution over the piecewise linear contact frame such that the moment will be zero at the frame nodes. In other words, given a certain contact frame node placement, one gets a solution for the contact forces that is a member of the set of all force distributions with zero moment at the frame nodes. Likewise, given a certain force distribution, one has to place the frame nodes such that Equations $(34)_{1,2}$ hold on all segments. This shows that given a set of patch test passing forces we have to place the frame nodes at their accompanying zero moment points is order to ensure that this set of forces will solve Equation (27). This completes the proof of the frame node placement proposition. □

Finally, we mention the special case that the moment line will be zero along the entire frame. This can only happen when the two sides have matching nodes and matching boundary interpolations. The frame node placement for such a case is trivial since the frame nodes have to be placed at the coinciding nodal positions of the contacting sides and the interpolation used between frame nodes becomes irrelevant. If the contacting body nodes do match, but the boundary interpolations do not, then a non-zero moment line with zero moment points exists and the zero moment rule can be used for frame node placement.

7.2. Non-singularity of contact enforcement operator

We have mentioned in the introduction of Section 7 that the number and placement of the frame nodes is of crucial importance for obtaining a system of equations that can be solved. This means in particular that Equation (28) has to define the frame displacements $\mathbf{v}$ uniquely and that Equation (27) has non-zero solutions for the localized Lagrange multipliers. The matrix $[\mathbf{L}_b^t\ \bar{\mathbf{L}}_b^t]$ determines whether we can meet these criteria.

Usage of frame node placement criterium (30) ensures that these criteria are satisfied. To demonstrate this, we need to show two properties of the zero moment rule first. For this purpose, consider two bodies in contact along a straight contact line. The constant normal stress field in these bodies produces collocated energy equivalent forces working on the contact frame as shown in Figure 9(a). The associated resultant normal force distribution along the frame line is shown in Figure 9(b). Since the forces are energy equivalent to the constant normal stress field in the two contacting bodies, they represent a set of patch test passing forces. The x locations of the contacting nodes of the two bodies are given at the bottom of the figure. The values of the collocated forces are given at the end points of the arrows. Further, the body node numbering is given right next to the frame for both sides. Starting from one side, find the location of the zero moment points along the frame, i.e. substitute the set of patch test passing forces into Equation (29) and solve Equation (30) for its roots x_s by sweeping from one end of the frame to the other. For example, the leftmost point in Figure 9 is the first zero moment point. The moment $M(x)$ (see Figure 7 for its sign convention) monotonously *decreases* (starting from 0 at the left side of the frame) until the resultant force changes sign, which happens at node 3. The moment then monotonously *increases* (starting from a negative value) until the next resultant force sign change at node $\bar{2}$. Hence, we can have at most one zero moment point between the nodes 3 and $\bar{2}$. Similar reasoning reveals

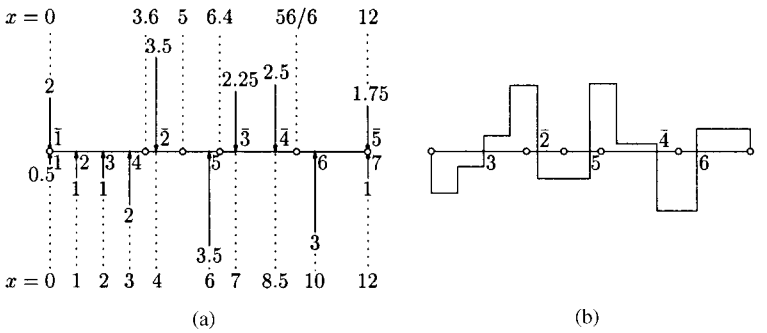

Figure 9. Limitation of the number of zero moment points by the number of resultant normal force sign changes: (a) representative patch test passing force system; and (b) resultant normal force distribution.

that the remaining zero moment points can occur only between the frame parts $\bar{2}$–5, 5–$\bar{4}$ and $\bar{4}$–6 with the final zero moment point occurring at the right end of the frame. The open dots in the figure give the actual locations of the zero moment points for this example, with their co-ordinates given at the top of the figure. We now offer the following observations

1. The upperbound to the number of zero moment points $(S+1)$ is

$$\text{upperbound of } S+1 = \text{number of resultant force sign changes } +1 \tag{36}$$

   This upperbound is always smaller than the total number of body nodes contacting from both sides of the frame.
2. The solutions x_s of Equation (30) for the zero moment point locations are *unique*.

Since the $S+1$ frame nodes are placed at a selection of the zero moment points, their number is limited and their location is *unique*. We now use the two properties listed above to motivate the non-singularity of our contact enforcement operator.

Equation (28) determines the frame displacements $\mathbf{v}$ uniquely if

$$\mathbf{L}_b^* = \begin{bmatrix} \mathbf{L}_b \\ \bar{\mathbf{L}}_b \end{bmatrix} = [c_1 \;\; c_2 \cdots c_{2S+2}] \tag{37}$$

has full column rank. The location of each frame node determines two columns of this matrix. We have observed already that the number of zero moment points is always smaller than the total number of body nodes contacting from both sides. Hence, the row size of matrix $\mathbf{L}_b^*$ is always larger than its column size. Moreover, we have seen that the zero moment point locations are unique. Therefore, the zero moment rule leads to an $\mathbf{L}_b^*$ matrix with independent columns, i.e. this frame construction gives a $\mathbf{L}_b^*$ with full column rank. The frame equilibrium equation (27) must have non-zero solutions for $(\boldsymbol{\lambda}, \bar{\boldsymbol{\lambda}})$. Otherwise, the formulation suffers from overconstraining. The zero moment rule ensures that the maximum number of frame nodes will be smaller than the total number of body nodes contacting the frame. Hence, the rows of $\mathbf{L}_b^*$ are not all independent and overconstraining the frame equilibrium equation does not occur.

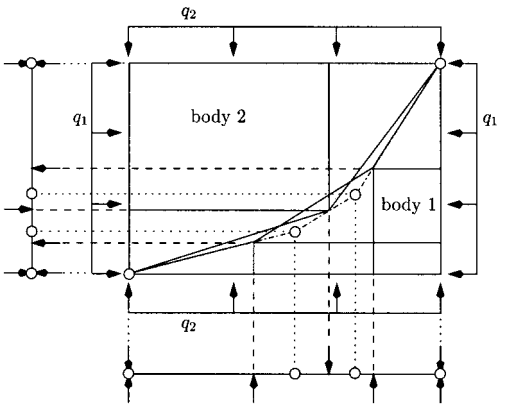

Figure 10. Projection method for the placement of contact frame nodes along a curved contact domain.

7.3. Frame nodal placement for non-planar contact surface

In general, the contact frame will be curved. The preceeding algorithm for node placement can be generalized to the case of a curved contact frame as indicated in Figure 10. This figure shows two discrete bodies in contact along a curved contact line. The bodies are loaded by a constant line load q_1 in horizontal direction and a constant line load q_2 in vertical direction. The objective now is to design the frame such that transfer of these loads takes places such that a constant stress state exists throughout the bodies. Frame equilibrium equation (22) can still be simplified to the form (34), but now one set of equations is obtained for the horizontal direction and one set for the vertical direction. This means that we have to work with the projection of the energy equivalent forces on the horizontal and vertical directions as indicated by the dashed lines for the inner body nodes in the figure. Then, we can compute the location of the zero moment points along each of the directions separately. The final step is to combine the found zero moment point locations in the two directions to obtain the patch test passing frame node positions. This process is illustrated by the dotted lines connecting the zero moment points (open dots) in the figure.

7.4. Discretization of frame slip displacement

The final issue in the construction of the discrete contact interface is the discretization of the slip displacement along the frame. In Section 6, we have shown that definition (9) leads to a frame positioning that is the average of the positions of the two contacting sides. In the discrete case we can enforce this average frame placement only at a distinct number of points. In essence, this means that when slip occurs along the whole frame, we have only a limited number of average frame placement constraints available that define the tangential motion of the frame. The maximum number of such constraints is set by the number of body nodes n in the coarser contact boundary. For the example shown in Figure 11 we can have a maximum of three average frame placement constraints that define up to three tangential frame displacement components uniquely. As a result, we can have a maximum of three frame nodes as indicated by the open dots in the figure. The frame nodes are chosen also as slip displacement nodes so that the slip field can be interpolated continuously along the frame.

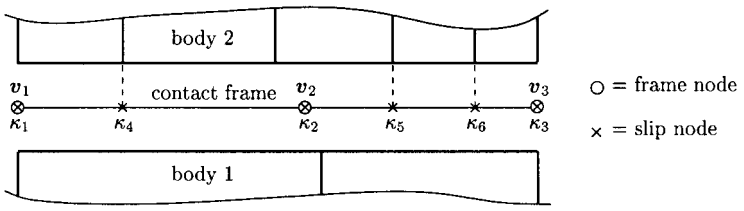

Figure 11. Slip displacement discretization.

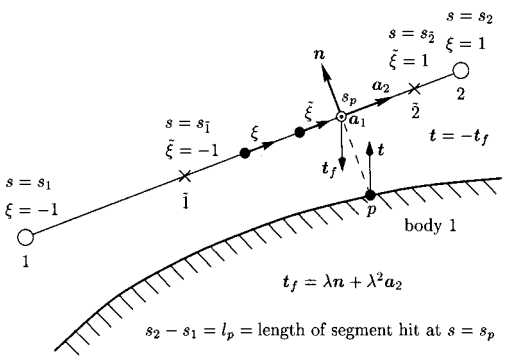

Figure 12. Expanded view of 2D contact between a linear contact frame segment and a mesh node p of contacting body 1.

Setting the number of frame nodes equal to m ($m \leqslant n$), we choose the m body nodes on either side of the frame that are closest to the frame nodes as the nodes that will define the average frame position during slip. Since this uniquely defines the tangential frame position, we can introduce additional slip nodes at the remaining body nodes in the contact boundary. For the example in Figure 11 we must have $m \leqslant 3$ and have chosen three frame nodes (placed at zero moment points). All three boundary nodes of body 1 and the three boundary nodes of body 2, that are closest to the frame nodes, are involved in defining the tangential motion of the frame. Then, we can choose the three remaining nodes in the contact boundary of body 2 to define three additional slip nodes as indicated by the dashed lines in the figure. We interpolate the slip displacement field linearly between the slip nodes.

8. DISCRETE FIRST VARIATION FOR 2D-CASE

Let us now consider the contact between a body node p and a linear contact frame segment, as shown in Figure 12. This pairing of a contact frame segment and a hitting node will be referred to as a *contact pair*. The entire contact of the two bodies simply becomes the union of all such pairs. A hitting node can be a member of only one such pair. A contact segment usually appears as a member of several contact pairs.

The position and displacements of the frame are interpolated linearly between the nodes 1 and 2 (open dots in Figure 12). The slip displacement is assumed to be interpolated linearly

between the nodes $\tilde{1}$ and $\tilde{2}$ (crosses in Figure 12). In general, slip displacement nodes will be placed at frame displacement nodes to maintain slip continuity between segments. The separate slip discretization simply allows additional slip nodes to be placed along the frame segment as explained in Section 7.4. Thus, the discretization along the frame segment is given by

$$\mathbf{Y}=\sum_{I=1}^{2} N_I \mathbf{Y}_I, \quad \mathbf{v}=\sum_{I=1}^{2} N_I \mathbf{v}_I, \quad \kappa_2=\sum_{I=1}^{2} N_{\tilde{I}} \kappa_{2\tilde{I}} \tag{38}$$

where

$$N_1=\tfrac{1}{2}(1-\xi), \quad N_2=\tfrac{1}{2}(1+\xi), \quad N_{\tilde{1}}=\tfrac{1}{2}(1-\tilde{\xi}), \quad N_{\tilde{2}}=\tfrac{1}{2}(1+\tilde{\xi})$$

$$\xi=\frac{1}{l_p}(2s-s_1-s_2) \quad \text{with } s_2>s_1 \quad \text{and} \quad -1\leqslant\xi\leqslant 1$$

in which l_p represents the *current* length of the contact frame segment and the s_I are the values of s at the end nodes of the contact frame segment. We choose contact co-ordinate ξ^2 to be the are length coordinate s.

Finally, to keep the contact interface generic, we stated already that the frame interacts with the bodies through a set of collocated forces at the nodal points of the contacting bodies. Mathematically, this can be represented by introducing a Dirac delta function δ such that

$$\int_{s_1}^{s_2} f(s)\delta(s-s_p)\,\mathrm{d}s=f(s_p) \tag{39}$$

where $\delta\to\infty$ for $s\to s_p$ and δ equal to zero outside an infinitesimal region around $s=s_p$. The components of the traction $\mathbf{t}_f$ defined over the contact segment of a contact pair are now defined by

$$\lambda(s)=\lambda_p\delta(s-s_p), \quad \lambda^2(s)=\lambda_p^2\delta(s-s_p) \tag{40}$$

Integrating this $\mathbf{t}_f$ over the contact segment results in a concentrated force $\lambda_p\mathbf{n}+\lambda_p^2\mathbf{a}_2$ applied at $s=s_p$.

To obtain the discrete form of the first variation, we first convert the integrations over the contact zones to summations over contact pairs. Hence, we write

$$\int_{\mathscr{A}_c}(\ldots)\,\mathrm{d}s=\sum_{p=1}^{P}\int_{l_p}(\ldots)\,\mathrm{d}s, \quad \int_{\bar{\mathscr{A}}_c}(\ldots)\,\mathrm{d}\bar{s}=\sum_{\bar{p}=1}^{\bar{P}}\int_{\bar{l}_{\bar{p}}}(\ldots)\,\mathrm{d}\bar{s}$$

in which capital P and $\bar{P}$ represent the total number of contact pairs on either side of the contact frame. Also, we need to define some finite element assembly operators in order to extract variables local to a specific contact pair from global vectors of unknowns. Therefore, we introduce

$$[\mathbf{u}]_p=\mathscr{L}_{up}\mathbf{u}, \quad \begin{bmatrix}\lambda\\ \lambda^2\end{bmatrix}_p=\mathscr{L}_{\lambda p}\boldsymbol{\lambda}, \quad \begin{bmatrix}\mathbf{v}_1\\ \mathbf{v}_2\end{bmatrix}_p=\mathscr{L}_{vp}\mathbf{v}, \quad \begin{bmatrix}\kappa_{2\tilde{1}}\\ \kappa_{2\tilde{2}}\end{bmatrix}_p=\mathscr{L}_{\kappa p}\boldsymbol{\kappa} \tag{41}$$

in which $\mathbf{u}$ is the vector of all structural nodal displacements on the non-barred side, $\boldsymbol{\lambda}$ the vector of all localized contact Lagrange multipliers on the non-barred side, $\mathbf{v}$ the vector of all contact frame nodal displacements and $\boldsymbol{\kappa}$ is the vector of all slip displacements. The operators $\mathscr{L}_{up}$, $\mathscr{L}_{\lambda p}$, $\mathscr{L}_{vp}$ and $\mathscr{L}_{\kappa p}$ are the Boolean finite element assembly operators. These select the unknowns local to a specific contact pair p from the global vectors of unknowns.

Substituting the discretization into expression (19) for $\delta\pi_c$ and carrying out the integrations, we arrive on the non-barred side at the following expression for the discrete form of the contact part of the first variation

$$\delta\pi_c = -\delta\mathbf{u}\cdot\mathbf{f}_c + \delta\boldsymbol{\lambda}\cdot\mathbf{g} - \delta\mathbf{v}\cdot\mathbf{p} + \delta\boldsymbol{\kappa}\cdot\mathbf{q} \tag{42}$$

where

$$\mathbf{f}_c = \sum_{p=1}^{P} \mathscr{L}_{up}^{t}\mathbf{f}_{cp}, \quad \mathbf{g} = \sum_{p=1}^{P} \mathscr{L}_{\lambda p}^{t}\mathbf{g}_p, \quad \mathbf{p} = \sum_{p=1}^{P} \mathscr{L}_{vp}^{t}\mathbf{p}_p, \quad \mathbf{q} = \sum_{p=1}^{P} \mathscr{L}_{\kappa p}^{t}\mathbf{q}_p$$

$$\mathbf{f}_{cp} = -\{\lambda\mathbf{n} + \lambda^2\mathbf{a}_2\}_p$$

$$\mathbf{g}_p = \left\{ \begin{bmatrix} \mathbf{n}\cdot(\mathbf{x}-\mathbf{y}) \\ \mathbf{a}_2\cdot(\mathbf{x}-\mathbf{y}) - \gamma\kappa_2 \end{bmatrix} \right\}_p$$

$$\mathbf{p}_p = \left\{ \begin{bmatrix} N_1\mathbf{I} \\ N_2\mathbf{I} \end{bmatrix} [\lambda\mathbf{n} + \lambda^2\mathbf{a}_2] - \begin{bmatrix} N_{1,2}\mathbf{I} \\ N_{2,2}\mathbf{I} \end{bmatrix} [\mathbf{Q}_2\boldsymbol{\Phi}^2(\mathbf{x}-\mathbf{y})] \right\}_p$$

$$\mathbf{q}_p = \left\{ \begin{bmatrix} N_{\tilde{1}} \\ N_{\tilde{2}} \end{bmatrix} [\gamma(\lambda_{\tilde{l}}^2 - \lambda^2) + (1-\gamma)\kappa^2] \right\}_p$$

The vector $\mathbf{f}_{cp}$ represents the contact-pair force acting on body 1. The vector $\mathbf{g}_p$ represents the contact-pair gap. The contact-pair force acting on the frame is represented by $\mathbf{p}_p$. Finally, $\mathbf{q}_p$ has two interpretations depending on whether or not the (constitutive) constraint on the frictional force is active. If it is active, i.e. when $\gamma = 1$, then it represents the constraint on the frictional force. Otherwise, i.e. when $\gamma = 0$, it sets the slip displacement equal to zero.

9. DISCRETE SECOND VARIATION FOR 2D-CASE

Using the frame-based contact first variation, as derived in the previous section, leads to a non-linear set of equations. This set of equations can be solved using a predictor–corrector scheme. The corrector consists of a sequence of Newton iterations, i.e. solving successive linearizations of the non-linear equations. In this section, we consider the linearization of the frame-based discrete contact first variation $\delta\pi_c^{\text{total}}$ (see Equation (19)). This leads to the so-called frame-based discrete contact second variation.

The linearization of $\delta\pi_c^{\text{total}}$ is obtained as follows. First, assume an arbitrary, but admissible, path through the configuration space given by

$$\begin{aligned}
\lambda(\eta) &= \lambda + \eta\Delta\lambda, \quad \bar{\lambda}(\eta) = \bar{\lambda} + \eta\Delta\bar{\lambda} \\
\lambda^2(\eta) &= \lambda^2 + \eta\Delta\lambda^2, \quad \bar{\lambda}^2(\eta) = \bar{\lambda}^2 + \eta\Delta\bar{\lambda}^2 \\
\mathbf{u}(\eta) &= \mathbf{u} + \eta\Delta\mathbf{u}, \quad \bar{\mathbf{u}}(\eta) = \bar{\mathbf{u}} + \eta\Delta\bar{\mathbf{u}} \\
\mathbf{v}(\eta) &= \mathbf{v} + \eta\Delta\mathbf{v}, \quad \bar{\mathbf{v}}(\eta) = \bar{\mathbf{v}} + \eta\Delta\bar{\mathbf{v}} \\
\kappa(\eta) &= \kappa + \eta\Delta\kappa, \quad \bar{\kappa}(\eta) = \bar{\kappa} + \eta\Delta\bar{\kappa}
\end{aligned} \tag{43}$$

in which η is the path parameter. Substitute the discretization presented in the previous section into path (43) and then substitute the obtained discrete admissible path into the frame-based discrete contact first variation. Finally, compute the linearization according to

$$L(\delta\pi_c^{\text{total}}) = \delta\pi_c^{\text{total}}\big|_{\eta=0} + \Delta\delta\pi_c^{\text{total}}, \quad \text{where} \quad \Delta\delta\pi_c^{\text{total}} = \left[\frac{d}{d\eta}\{\delta\pi_c^{\text{total}}(\eta)\}\right]\Bigg|_{\eta=0} \tag{44}$$

After straightforward manipulations we arrive on the non-barred side at the following expression for the frame-based discrete contact second variation

$$\begin{aligned}
\Delta\delta\pi_c = {} & \delta\mathbf{u}\cdot\{\mathbf{B}\Delta\boldsymbol{\lambda} - \mathbf{L}_v\Delta\mathbf{v}\} + \delta\boldsymbol{\lambda}\cdot\{\mathbf{B}^t\Delta\mathbf{u} - \mathbf{L}_b\Delta\mathbf{v} - \mathbf{L}_\kappa\Delta\boldsymbol{\kappa}\} \\
& + \delta\mathbf{v}\cdot\{-\mathbf{L}_v^t\Delta\mathbf{u} - \mathbf{L}_b^t\Delta\boldsymbol{\lambda} - \mathbf{D}_v\Delta\mathbf{v}\} + \delta\boldsymbol{\kappa}\cdot\{-\mathbf{L}_\kappa^t\Delta\boldsymbol{\lambda} + \mathbf{D}_\kappa\Delta\boldsymbol{\kappa}\}
\end{aligned} \tag{45}$$

where

$$\mathbf{B} = \sum_{p=1}^{P} \mathscr{L}_{up}^t\mathbf{B}_p\mathscr{L}_{\lambda p}, \quad \mathbf{L}_v = \sum_{p=1}^{P} \mathscr{L}_{up}^t\mathbf{L}_{vp}\mathscr{L}_{vp}, \quad \mathbf{L}_b = \sum_{p=1}^{P} \mathscr{L}_{\lambda p}^t\mathbf{L}_{bp}\mathscr{L}_{vp}$$

$$\mathbf{L}_\kappa = \sum_{p=1}^{P} \mathscr{L}_{\lambda p}^t\mathbf{L}_{\kappa p}\mathscr{L}_{\kappa p}, \quad \mathbf{D}_v = \sum_{p=1}^{P} \mathscr{L}_{vp}^t\mathbf{D}_{vp}\mathscr{L}_{vp}, \quad \mathbf{D}_\kappa = \sum_{p=1}^{P} \mathscr{L}_{\kappa p}^t\mathbf{D}_{\kappa p}\mathscr{L}_{\kappa p}$$

$$\mathbf{B}_p = \{[\mathbf{n} \quad \mathbf{a}_2]\}_p$$

$$\mathbf{L}_{vp} = \{[-(\boldsymbol{\Phi}^2)^t\mathbf{Q}_2][N_{1,2}\mathbf{I} \;\; N_{2,2}\mathbf{I}]\}_p$$

$$\mathbf{L}_{bp} = \left\{\begin{bmatrix}\mathbf{n}^t \\ \mathbf{a}_2^t\end{bmatrix}[N_1\mathbf{I} \;\; N_2\mathbf{I}] - \begin{bmatrix}(\mathbf{x}-\mathbf{y})^t(\mathbf{a}_1\times\mathbf{I}) \\ (\mathbf{x}-\mathbf{y})^t\end{bmatrix}\mathbf{Q}_2[N_{1,2}\mathbf{I} \;\; N_{2,2}\mathbf{I}]\right\}_p$$

$$\mathbf{L}_{\kappa p} = \left\{\begin{bmatrix}0 \\ \gamma\end{bmatrix}[N_{\tilde{1}} \;\; N_{\tilde{2}}]\right\}_p$$

$$\mathbf{D}_{vp} = \left\{ \begin{bmatrix} N_1\mathbf{I} \\ N_2\mathbf{I} \end{bmatrix} [(\boldsymbol{\Phi}^2)^{\mathrm{t}}\mathbf{Q}_2][N_{1,2}\mathbf{I} \;\; N_{2,2}\mathbf{I}] + \begin{bmatrix} N_{1,2}\mathbf{I} \\ N_{2,2}\mathbf{I} \end{bmatrix} [\mathbf{Q}_2\boldsymbol{\Phi}^2][N_1\mathbf{I} \;\; N_2\mathbf{I}] \right.$$
$$+ \begin{bmatrix} N_{1,2}\mathbf{I} \\ N_{2,2}\mathbf{I} \end{bmatrix} \frac{1}{\|\mathbf{y}_{,2}\|}([\mathbf{Q}_2\boldsymbol{\Phi}^2(\mathbf{x}-\mathbf{y})] \otimes \mathbf{a}_2 + \mathbf{a}_2 \otimes [\mathbf{Q}_2\boldsymbol{\Phi}^2(\mathbf{x}-\mathbf{y})]$$
$$\left. + \{[\boldsymbol{\Phi}^2(\mathbf{x}-\mathbf{y})] \cdot \mathbf{a}_2\}\mathbf{Q}_2)[N_{1,2}\mathbf{I} \;\; N_{2,2}\mathbf{I}] \right\}_p = \mathbf{D}_{vp}^{\mathrm{t}}$$

$$\mathbf{D}_{\kappa p} = \left\{ \begin{bmatrix} N_{\bar{1}} \\ N_{\bar{2}} \end{bmatrix} (1-\gamma)[N_{\bar{1}} \quad N_{\bar{2}}] \right\}_p = \mathbf{D}_{\kappa p}^{\mathrm{t}}$$

in which the $\Delta\mathbf{u}$ and $\Delta\mathbf{v}$ are aggregate variables storing increment vectors at all body (for non-barred side) and frame nodes as opposed to their meaning in Equation (43) as being displacement increment vectors of a single point. The frame-based discrete contact first and second variations on the barred side follow also from expressions (42) and (45) by following the contact frame in the opposite direction.

We write the linearization of the first variation of the potential energy of the body on the non-barred side in the form

$$\delta\pi_{\mathrm{free}}^{\mathrm{total}} = \delta\mathbf{u} \cdot (\mathbf{f} + \mathbf{K}\Delta\mathbf{u}) \quad \text{with } \mathbf{K} = \frac{\partial \mathbf{f}}{\partial \mathbf{u}} \tag{46}$$

and note that $\mathbf{f} = \mathbf{0}$ are its non-linear equilibrium equations. The matrix $\mathbf{K}$ represents its stiffness matrix. A similar expression describes the behaviour of the body on the barred side. We now write the Newton system of equations of the frame-based contact problem as

$$\begin{bmatrix} \mathbf{K} & \mathbf{0} & \mathbf{B} & \mathbf{0} & -\mathbf{L}_v & \mathbf{0} \\ \mathbf{0} & \bar{\mathbf{K}} & \mathbf{0} & \bar{\mathbf{B}} & -\bar{\mathbf{L}}_v & \mathbf{0} \\ \mathbf{B}^{\mathrm{t}} & \mathbf{0} & \mathbf{0} & \mathbf{0} & -\mathbf{L}_b & -\mathbf{L}_\kappa \\ \mathbf{0} & \bar{\mathbf{B}}^{\mathrm{t}} & \mathbf{0} & \mathbf{0} & -\bar{\mathbf{L}}_b & -\bar{\mathbf{L}}_\kappa \\ -\mathbf{L}_v^{\mathrm{t}} & -\bar{\mathbf{L}}_v^{\mathrm{t}} & -\mathbf{L}_b^{\mathrm{t}} & -\bar{\mathbf{L}}_b^{\mathrm{t}} & -\mathbf{D}_v - \bar{\mathbf{D}}_v & \mathbf{0} \\ \mathbf{0} & \mathbf{0} & -\mathbf{L}_\kappa^{\mathrm{t}} & -\bar{\mathbf{L}}_\kappa^{\mathrm{t}} & \mathbf{0} & \mathbf{D}_\kappa + \bar{\mathbf{D}}_\kappa \end{bmatrix} \begin{bmatrix} \Delta\mathbf{u} \\ \Delta\bar{\mathbf{u}} \\ \Delta\boldsymbol{\lambda} \\ \Delta\bar{\boldsymbol{\lambda}} \\ \Delta\mathbf{v} \\ \Delta\boldsymbol{\kappa} \end{bmatrix} = \begin{bmatrix} -\mathbf{f} + \mathbf{f}_{\mathrm{c}} \\ -\bar{\mathbf{f}} + \bar{\mathbf{f}}_{\mathrm{c}} \\ -\mathbf{g} \\ -\bar{\mathbf{g}} \\ \mathbf{p} + \bar{\mathbf{p}} \\ -\mathbf{q} - \bar{\mathbf{q}} \end{bmatrix} \tag{47}$$

A significant feature of our frame-based contact model is immediately visible from these equations, namely, they are symmetric. This is due to the fact that every contact node is treated in exactly the same way, namely, the gap constraint and the collocated force continuity are enforced between every body contact node and the frame. This is in sharp contrast with the contact formulations proposed in References [12, 13, 16] which result in a set of non-symmetric Newton equations that can be represented by

$$\begin{bmatrix} \mathbf{K} & \mathbf{B} \\ \mathbf{C}^{\mathrm{t}} & \mathbf{0} \end{bmatrix} \begin{bmatrix} \Delta\mathbf{u} \\ \Delta\boldsymbol{\lambda} \end{bmatrix} = \begin{bmatrix} -\mathbf{f} + \mathbf{f}_{\mathrm{c}} \\ -\mathbf{g} \end{bmatrix} \tag{48}$$

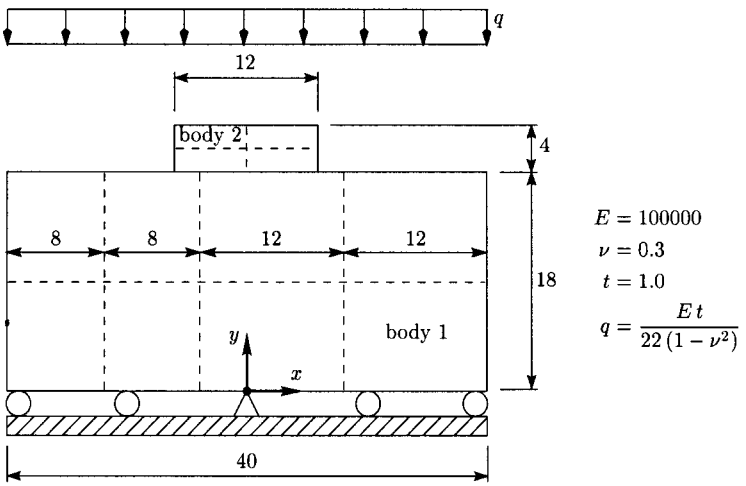

Figure 13. Plane strain contact patch test problem.

with **C** in general not equal to **B** and **u**, **λ** being discrete representative body displacements and Lagrange multipliers. In contrast, our frame-based formulation results in a symmetric system of iterative equations which is a definite advantage for solving the equations.

The contact frame node placement depends on the place of the body nodes that come into contact. The system of equations to solve in one load or time step is non-linear and requires a number of Newton iterations for obtaining the solution with acceptable tolerance. This means that each Newton iteration results in a change in the contact boundary deformation and possibly also sliding, so that the position of the body nodes in contact will change. Hence, before each additional Newton iteration, one has to recompute the zero moment points and reconstruct the contact frame. This can be seen as a pre-processing step before each Newton iteration.

10. NUMERICAL SIMULATIONS

Three numerical examples are presented. The first two are intended to demonstrate the ability of our formulation to transfer constant stress states correctly through the contact frame. The first example is a contact patch test taken from literature. In the second example, we will include frictionless sliding. The third example looks at the 2D-contact of a pin in a hole in a plate. It has a curved contact frame as opposed to the flat contact frame of the first two examples.

10.1. Contact patch test

A flexible punch comes into contact with a deformable foundation as in Figure 13. Uniform loading q is applied on the free upper surface of both the punch and the foundation. Plane strain and linear elasticity are assumed. The same elastic constants are used in the computations for both bodies and they are given in the figure. The thickness t of both bodies is taken

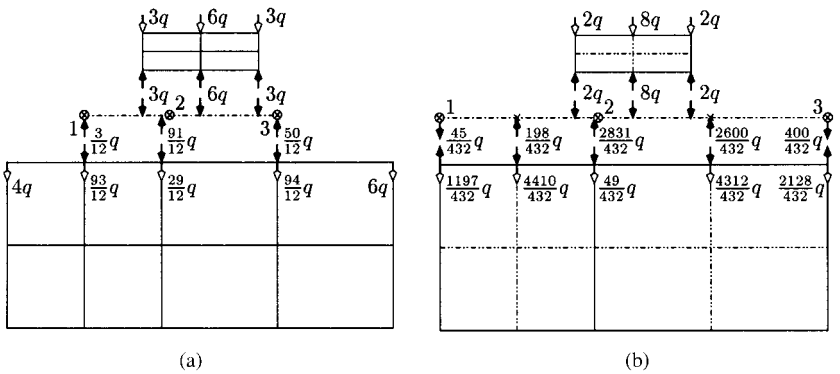

Figure 14. Applied (energy equivalent) load system and computed collocated contact forces that act on the deformed bodies for a non-matching mesh (four-noded bilinear elements are used in (a), while nine-noded quadratic elements are used in (b)).

to be 1.0. The dimensions are given in the figure. The boundary conditions allow for free lateral expansion. This problem tests the capability of our formulation to allow transmission of constant pressure through the contact surface. The same problem was used by Papadopoulos and Taylor [9, 17] for this purpose.

The computations were performed using the mesh that is shown with dashed lines in Figure 13. The mesh of body 2 is regular in both directions. The mesh of body 1 is taken regular in the vertical direction. Its meshing in horizontal direction is given in the figure. Four-noded plane strain quads were used for case (a), whereas nine-noded plane strain quads were used in case (b). Please notice that the mesh set-ups are non-matching at the contact surface. This is an essential characteristic of the contact patch test. The distributed line load q is cast into a set of energy equivalent forces which are applied to the nodal points of the loaded edges. These forces are given by open arrows in Figure 14. We would like to note that the elements of the foundation, that are in contact with the punch, are only partly loaded by line load q on their top surface. This has been taken into account in the computation of the energy equivalent forces.

The value for the distributed line load q has been selected such that the top of body 2 displaces 1 downward. To obtain the corresponding expression for q, we first note that the stress state (in both bodies) is given by

$$\sigma_x = 0, \quad \sigma_y = -\frac{q}{t}, \quad \tau_{xy} = 0$$

The corresponding plane strain state is

$$\varepsilon_x = \frac{-\nu(1+\nu)}{E}\sigma_y, \quad \varepsilon_y = \frac{(1-\nu)(1+\nu)}{E}\sigma_y, \quad \gamma_{xy} = 0$$

The condition $\varepsilon_y = -1/22$ then leads to

$$q = \frac{Et}{22(1-\nu^2)}$$

Table I. Computed internal energy.

Case	(a)	(b)
U^1	81736.445373	81736.445373
U^2	5449.096358	5449.096358

Table II. Final contact frame node positions.

	Case (a)		Case (b)	
Frame node	x	y	x	y
1	−12.233766	17.181818	−20.389610	17.181818
2	−3.234214	17.181818	−3.662436	17.181818
3	8.155844	17.181818	20.389610	17.181818

as the load to use to get a downward displacement of unity at the top of body 2. The internal energy in each of the bodies is computed from

$$U^\alpha = \frac{1}{2}\sigma_y \varepsilon_y V^\alpha = \frac{(1-\nu^2)}{2E}\left(\frac{q}{t}\right)^2 V^\alpha \quad \text{with } \alpha = 1,2$$

in which V^α represents the volume of body α.

The computation results for the contact forces acting on the contact frame are drawn in the exploded view of the deformed state plotted in Figure 14. These forces are represented by filled arrows. By adding the forces applied to the top nodes of body 1 and the contact forces acting on this body, one verifies easily that the result exactly corresponds to the energy equivalent forces that belong to a constant stress state in body 1. The computed contact forces acting on body 2 are the energy equivalent forces belonging to a constant stress state in body 2.

The internal energy in the two bodies has been computed for the two cases and the results are reported in Table I. These results are in perfect agreement with the theoretical values.

The final position of the contact frame nodes is given in Table II. The node numbers in this table refer to the contact frame node numbering in Figure 14. It is easily verified that each of these nodes is situated at a zero moment point. The downward displacement of the top of body 1 is equal to $18 \cdot \varepsilon_y = 0.818182$ so that the final y-co-ordinate of the frame must be 17.181818, which is equal to the computed value. Since the minimum number of body nodes in the contact domain on one side is 3, the maximum number of frame nodes (open dots in the figure) for which we can define the tangential motion is 3. Slip nodes are placed at the frame nodes (crosses in the figure). For case (b) we have more than three foundation nodes in the contact domain so that two additional slip nodes have been defined for this case.

Finally, we note that the computational results were obtained in a single Newton iteration step. This is because no sliding has to take place since the Poisson ratios of the two contacting bodies are equal. We conclude that the numerical results are in perfect agreement

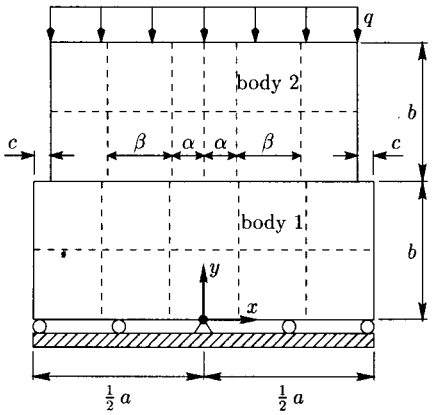

$$a = 5 \;;\; b = 2 \;;\; c = 0.25$$

$$E = 216 \;;\; t = 1$$

body 1: $E^1 = E \;;\; \nu^1 = 0.1 \;;\; t^1 = t$

body 2: $E^2 = E \;;\; \nu^2 = 0.3 \;;\; t^2 = t$

$$q = \frac{2Etc}{\{\nu^2(1+\nu^2) - \nu^1(1+\nu^1)\}(a-2c)}$$

$$\varepsilon_x^1 = \frac{\nu^1(1+\nu^1)(a-2c)q}{Eat}$$

$$\varepsilon_x^2 = \frac{\nu^2(1+\nu^2)q}{Et}$$

$$\alpha = \frac{a(2+\varepsilon_x^1)}{10(2+\varepsilon_x^2)} \;;\; \beta = \frac{2a(2+\varepsilon_x^1)}{10(2+\varepsilon_x^2)}$$

Figure 15. Plane strain contact patch test problem with sliding.

with the theoretically expected behaviour. Therefore, our formulation passes the contact patch tests.

10.2. Contact patch test with sliding

The contact patch test presented in the previous section did not involve any sliding. The plane strain test problem shown in Figure 15 is specifically designed to include this aspect in the computations. Two bodies come into static contact. The top body carries a distributed line load q on one side and is supported by a flexible body on the other side. The contact between the bodies is assumed to be frictionless. The bodies have different and non-zero Poisson ratios. This way, relatively sliding with respect to the contact frame will take place for each body. The lower body rests on a rigid foundation and its support allows it to expand freely in the x-direction. The load q is chosen such that the width of the two bodies becomes equal after deformation. Hence, the analysis should yield a constant stress state in each body. The thickness and elasticity modulus are the same in both bodies. Numerical values for the material parameters as well as the problem dimensions are given in the figure.

Figure 15 also shows the finite element mesh. Four-noded plane strain elements were used. The mesh of body 1 is regular in both directions. The meshing of body 2 is regular only in the vertical direction. The details of the horizontal meshing of body 2 can be found in the figure. The meshing has been designed such that four mesh lines of body 2 will slide beyond vertical mesh lines of body 1 and that the horizontal distance to the mesh lines they pass is the same in the initial and deformed states. The meshing of body 2 is symmetric will respect to the y-axis.

The value for the distributed line load q has been selected such that the width of the two bodies becomes equal after deformation. To obtain the corresponding value for q, we first note that the stress state is intended to become

$$\sigma_x^\alpha = 0, \quad \sigma_y^1 = -\frac{q(a-2c)}{at} \quad \text{and} \quad \sigma_y^2 = -\frac{q}{t}, \quad \tau_{xy}^\alpha = 0 \quad \text{with } \alpha = 1,2$$

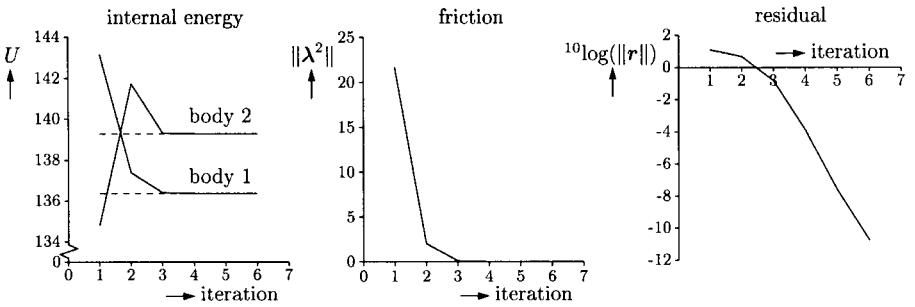

Figure 16. Newton iteration convergence behaviour.

in which a superindex is used as body index. The corresponding plane strain state is given by

$$\varepsilon_x^1 = \frac{v^1(1+v^1)(a-2c)q}{Eat}, \quad \varepsilon_y^1 = -\frac{(1-v^1)(1+v^1)(a-2c)q}{Eat}, \quad \gamma_{xy}^1 = 0$$

$$\varepsilon_x^2 = \frac{v^2(1+v^2)q}{Et}, \quad \varepsilon_y^2 = -\frac{(1-v^2)(1+v^2)q}{Et}, \quad \gamma_{xy}^2 = 0$$

The condition that the width of the two bodies becomes equal after deformation can now be written as

$$(1+\varepsilon_x^1)a = (1+\varepsilon_x^2)(a-2c)$$

and yields the formula for q that is given in Figure 15. As stated earlier, the meshing is designed such that vertical mesh lines of the top and bottom bodies will pass each other at the contact surface. To ensure this, we require that the horizontal distance between passing mesh lines is the same in the initial and deformed states. This requirement can be written as

$$\left(\frac{a}{10} - \alpha\right) = (1+\varepsilon_x^2)\alpha - (1+\varepsilon_x^1)\frac{a}{10}$$

$$\left(\frac{3a}{10} - \alpha - \beta\right) = (1+\varepsilon_x^2)(\alpha+\beta) - (1+\varepsilon_x^1)\frac{3a}{10}$$

and leads to the expressions for α and β that are given in Figure 15. The internal energy in each of the bodies is computed from

$$U^\alpha = \tfrac{1}{2}\sigma_y^\alpha \varepsilon_y^\alpha V^\alpha \quad \text{with } \alpha = 1,2$$

in which V^α represents the volume of body α.

The problem to solve in inherently non-linear. A total number of six Newton iteration steps were performed. In the first step, all contact points are assumed to be in a stick state. All the other steps (2–6) are performed using a slip state at all the contact points.

The convergence behaviour of the algorithm is illustrated in Figure 16. The horizontal axis shows the number of Newton iteration steps. The horizontal dashed lines indicate the theoretical values for the internal energy in each of the bodies. The symbol $\|\lambda^2\|$ at the vertical

Table III. Computed internal energy and friction norm at the final iteration step.

	U^1	U^2	$\|\lambda^2\|$
Iteration 6	136.377551	139.285714	8.1877e-07
Theoretical	136.377551	139.285714	0

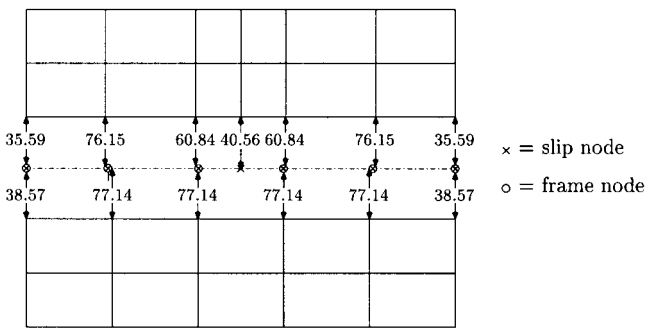

Figure 17. Exploded view of the final deformation which shows the contact frame location and the contact forces.

axis of the friction figure represents the norm of a vector in which all frictional contact forces are collected. The residual is defined as the right-hand side vector of Equation (47), i.e. the error in the first variation, and should converge to zero. All the three plots show rapid convergence. The final values computed for the internal energy and the frictional forces norm at the last iteration step are given in Table III. The agreement with the theoretical values is excellent.

Finally, let us take a closer look at the behaviour of the contact frame. Figure 17 shows an exploded view of the final deformed state. The contact frame is drawn in between the two bodies and the computed contact forces are also given. It is easily verified that these forces correspond exactly to the energy equivalent forces that belong to the constant stress states in the two bodies. This figure also shows that six frame nodes were used. Six slip nodes are placed at the frame nodes and one additional slip node was introduced at the centre of the frame.

The behaviour of the contact frame during iterations can be found in Figure 18. Observe from this figure that the frame nodes do move during iterations in order for the nodes to lie at zero moment positions, a key requirement to pass the contact patch test in the present formulation.

A number of conclusions can be drawn from the presented results for this example. In the first place, we note that the algorithm converges to the theoretically expected behaviour. Secondly, convergence occurs in a low number of iterations. This example shows also that mesh lines that pass each other at the contact surface do not pose any problems. Nodes on opposing sides of the contact frame that need to pass each other are detected and taken care

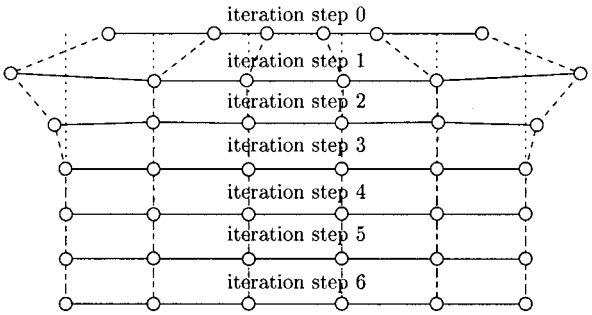

Figure 18. Movement of frame nodes during iterations in order for the nodes to be placed at zero moment positions. The horizontal motion is magnified by five times to illustrate the importance of frame nodal adjustments.

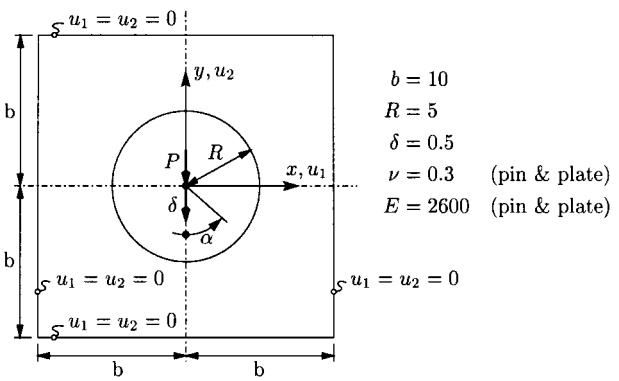

Figure 19. Two-dimensional contact of a pin in a hole in a plate. The unloaded pin and hole have the same radius.

of, while the frame node positions are adapted to be at zero moment positions. This proves to be working well.

10.3. Two-dimensional contact of a pin in a hole in a plate

We now turn to a problem that has a curved contact frame as opposed to the flat contact frame of the first two numerical examples and look at the 2D-contact of a pin in a hole in a plate. Figure 19 shows a circular pin in contact with a circular hole in a plate. Both the pin and hole have radius R, i.e. there is no clearance nor interference between the pin and plate in the unloaded state. The clamped boundary conditions suppress all displacements along the outside boundary of the plate. The external load P is applied to the pin effectively at its centre and causes its centre to displace δ downward. The meshes of the pin and plate match in the reference configuration as shown in Figure 20(a). The frame nodes then match the nodal positions on either side of the contact frame (open dots in the figure). The slip nodes are placed at the frame nodes (crosses in the figure). Four-noded plane strain elements were used in the analysis.

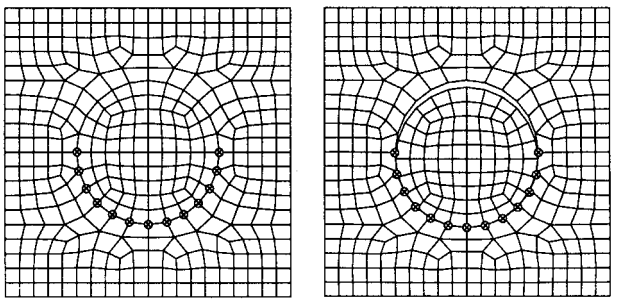

Figure 20. (a) Discretization in the reference configuration; and (b) deformation at final iteration (iteration 8).

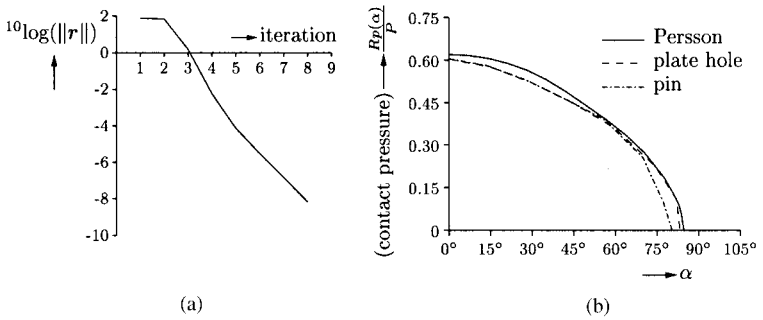

Figure 21. (a) Newton convergence behaviour; and (b) normal pressure distribution $p(\alpha)$ in the contact domain.

A total of eight Newton iteration steps were carried out. The first step used a stick state at all contacting nodes. The other steps used a slip state throughout the model. Rapid Newton convergence behaviour is obtained as shown in Figure 21(a) in which the residual r is defined as the right-hand side vector of equation (47). The final deformed state at iteration 8 is shown in Figure 20(b). Observe that the body nodes are no longer matching in the contact domain. The location of the frame nodes has been adapted before each Newton iteration step to place them at zero moment points. A pressure distribution has been generated from the collocated contact forces at each side of the contact frame. The results are given in Figure 21(b) and compared to the normal pressure distribution obtained by Persson [32, 33]. The normal pressure distribution obtained for the pin and plate are nearly coinciding except at the very end. The mesh is too coarse to resolve the end of the contact domain with high precision. Deviations from Persson's results are to be expected since the plate in this example is finite, while Persson's results hold for an infinite plate. The finite dimensions of the plate cause the boundary conditions to become important. To study their influence we repeated the computation with a set of boundary conditions that allow free lateral expansion. This means that the top and bottom faces of the plate are allowed to slide freely in horizontal

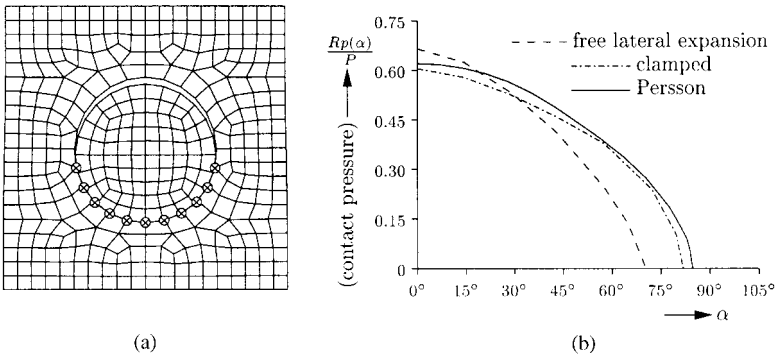

Figure 22. (a) Deformation when boundary conditions allow free lateral expansion; and (b) influence of the boundary conditions on the normal pressure distribution $p(\alpha)$ in the contact domain.

direction. The left and right outer boundaries are left completely free. We expect the pressure distribution to concentrate more around $\alpha = 0$ accompanied by a shorter contact domain as a result of the fact that the resistance for the plate to move sideways is reduced. Figure 22 shows the computational results. Indeed, the frame is shorter and the number of frame nodes is reduced by two. The average of the computational results for the pressure distribution on both sides of the frame is shown in Figure 22(b) for both boundary condition sets. The pressure is indeed more concentrated around $\alpha = 0$. Moreover, the pressure predicted by Persson at $\alpha = 0$ is in between our computational results. This can be expected since the boundary conditions that should be used to simulate the infinite plate behaviour with our finite plate model are in between the two sets we used. Finally, we conclude that we get satisfactory agreement of our numerical results with Persson's results.

11. CONCLUSION

We have introduced a novel element in the modelling of contact problems, namely, an adaptive contact frame placed in between contacting bodies. The contact frame is endowed with its independent displacements and the associated equilibrium equations. The contact becomes indirect because the contact forces are exerted on the contact frame and not directly from one body onto the other. A number of advantages can be mentioned. First, our formulation yields a variationally consistent force equilibrium equation for the contact frame. This ensures force equilibrium in the contact domain even for discrete contact models. Basically, it takes care of the problem of *non-matching* meshes of the contacting bodies in a consistent manner. Second, all integrations at one side of the contact frame are completely *localized* to that side of the contact frame. This property makes it possible to design a *stand-alone* and *modular* contact frame by requiring that only nodal information from the contacting bodies is used in the construction of the frame. We regard this property as most important in our formulation. It implies that any finite element program can be used to generate the nodal information. The stand-alone contact interface is then used as a module to handle the contact enforcement. Third, the introduction of

the tangential motion of the contact frame allows to model frictional contact from the outset of the present formulation.

For the case of 2D-contact we have shown that it is possible to design the contact interface such that it can transfer constant stress states exactly. Numerical examples have been used to demonstrate this ability. Future work needs to focus on the 3D-case. Like in the 2D-case a method needs to be found for designing the 3D-contact frame such that it can transfer constant stress states exactly.

ACKNOWLEDGEMENTS

The present work has been supported by Sandia National Laboratories under the Accelerated Strategic Computational Initiative (ASCI) contract AS-5666 and by Lawrence Livermore National Laboratories under the Scalable Algorithms for Massively Parallel Computations (ASCI level-II) contract B347880.

REFERENCES

1. Chan SK, Tuba IS. A finite element method for contact problems of solid bodies: I. theory and validation. *International Journal of Mechanical Sciences* 1971; **13**:627–639.
2. Francavilla A, Zienkiewicz OC. A note on numerical computation of elastic contact problems. *International Journal for Numerical Methods in Engineering* 1975; **9**:913–924.
3. Hughes TJR, Taylor RL, Sackman JL, Curnier A, Kanoknukulchai W. A finite element method for a class of contact-impact problems. *Computer Methods in Applied Mechanics and Engineering* 1976; **8**:249–276.
4. Valliappan S, Lee IK, Boonlualohr P. Non-linear analysis of contact problems. In *Numerical Methods in Coupled Systems*, Lewis RW, Bettess P, Hinton E (eds). Wiley: New York, 1984.
5. Zhong ZH. *Finite Element Procedures for Contact-Impact Problems*. Oxford University Press: Oxford, 1993.
6. Kikuchi N, Oden JT. Contact problems in elastostatics. In *Finite Elements*: *Special Problems in Solid Mechanics*, vol. IV, Oden JT, Carey GF (eds). Prentice-Hall: Engelwood Cliffs, NJ, 1984.
7. Oden JT. Exterior penalty methods for contact problems in elasticity. In *Nonlinear Finite Element Analysis in Structural Mechanics*, Bathe KJ, Stein E, Wunderlich W (eds). Springer: Berlin, 1980.
8. McDevitt TW, Laursen TA. A mortar-finite element formulation for frictional contact problems. *International Journal for Numerical Methods in Engineering* 2000; **48**:1525–1547.
9. Papadopoulos P, Taylor RL. A mixed formulation for the finite element solution of contact problems. *Computer Methods in Applied Mechanics and Engineering* 1992; **94**:373–389.
10. Simo JC, Wriggers P, Taylor RL. A perturbed Lagrangian formulation for the finite element solution of contact problems. *Computer Methods in Applied Mechanics and Engineering* 1985; **50**:163–180.
11. Papadopoulos P, Jones RE, Solberg JM. A novel finite element formulation for frictionless contact problems. *International Journal for Numerical Methods in Engineering* 1995; **38**:2603–2617.
12. Papadopoulos P, Solberg JM. A Lagrange multiplier method for the finite element solution of frictionless contact problems. *Mathematical and Computer Modelling* 1998; **28**:373–384.
13. Jones RE, Papadopoulos P. A yield-limited Lagrange multiplier formulation for frictional contact. *International Journal for Numerical Methods in Engineering* 2000; **48**:1127–1149.
14. Bernardi C, Maday Y, Patera AT. A new nonconfirming approach to domain decomposition: the mortar element method. *Technical Report*, Université Pierre at Marie Curie, Paris, France, 1990.
15. Belgacem FB, Hild P, Laborde P. Approximation of the unilateral contact problem by the mortar finite element method. *ComptesRendus de L'Académie des Sciences* 1991; **324**:123–127.
16. Crisfield MA. Re-visiting the contact patch test. *International Journal for Numerical Methods in Engineering* 2000; **48**:435–449.
17. Taylor RL, Papadopoulos P. On a patch test for contact problems in two dimensions. In *Nonlinear Computational Mechanics*, Wriggers P, Wagner W (eds). Springer: Berlin, 1991; 690–702.
18. Park KC, Felippa CA. A variational framework for solution method developments in structural mechanics. *Journal of Applied Mechanics* 1998; **65**:242–249.
19. Park KC, Felippa CA. A variational principle for the formulation of partitioned structural systems. *International Journal for Numerical Methods in Engineering* 2000; **47**:395–418.
20. Justino MR, Park KC, Felippa CA. An algebraic partitioned FETI method for parallel structural analysis: implementation and numerical performance evaluation. *International Journal for Numerical Methods in Engineering* 1997; **40**:2739–2758.

21. Alvin KF, Park KC. Extraction of substructural flexibility from measured global frequencies and mode shapes. *Proceedings of the 1996 AIAA SDM Conference*, Salt Lake City, UT, April 15–16, Paper No. AIAA 96-1297, 1996.
22. Aminpour MA, Krishnamurthy T, Fadale TD. Coupling of independently modelled three-dimensional finite element meshes with arbitrary shape interface boundaries. *Proceedings of the 1998 AIAA SDM Conference*, Paper No. AIAA 98-2060, 1998; 3014–3024.
23. Zhong ZH. On numerical procedure for contact problems. *Licentiate Thesis*, 1987:02L, Luleå University, Luleå, 1987.
24. Nilsson L, Zhong ZH. High performance numerical algorithms for the evaluation of general contact-impact interface. *Proceedings of the Post-SMiRT Seminar Impact III*, Tokyo, 1991.
25. Benson BJ, Hallquist JO. A single surface contact algorithm for the post-buckling analysis of structures. *Computer Methods in Applied Mechanics and Engineering* 1990; **78**:141–163.
26. Heinstein MW, Attaway SW, Swegle JW, Mello FJ. A general-purpose contact detection algorithm for nonlinear structural analysis codes. Sandia National Laboratories, *Report* SAND92-2141. Albuquerque, New Mexico, 1995.
27. Casey J. On finitely deforming rigid-plastic materials. *International Journal of Plasticity* 1986: **2**:247–277.
28. Kikuchi N, Oden JT. *Contact Problems in Elasticity*: *A Study of Variational Inequalities and Finite Element Methods*. SIAM Studies in Applied Mathematics, vol. 8. SIAM: Philadelphia, PA, 1988.
29. Zienkiewicz OC, Qu S, Taylor RL, Nakazawa S. The patch test for mixed formulations. *International Journal for Numerical Methods in Engineering* 1986; **23**:1873–1883.
30. Park KC, Felippa CA, Rebel G. Interfacing nonmatching FEM meshes: the zero moment rule. In *Trends in Computational Structural Mechanics*, Wall WA, Bletzinger KU, Schweizerhof K (eds). International Center for Numerical Methods in Engineering: Barcelona, 2001: 355–367.
31. Park KC, Felippa CA, Rebel G. A simple algorithm for localized construction of non-matching structural interfaces. *International Journal for Numerical Methods in Engineering* 2002; **53**:2117–2142.
32. Persson A. On the stress distribution of cylindrical elastic bodies in contact. *Dissertation*, Chalmers Tekniska Hogskola, Göteborg, 1964.
33. Johnson KL. *Contact Mechanics*. Cambridge University Press: Cambridge, 1985.

